AD-A093 480 ENVIRONMENTAL RESEARCH INST OF MICHIGAN ANN ARBOR F/G 19/5
HOLOGRAPHIC IMAGING THROUGH SCATTERING MEDIA.(U)
OCT 80 A M TAI, C C ALEKSOFF DAAK11-79-C-0073
UNCLASSIFIED ERIM-143400-4-F ARBRL-CR-00439 NL

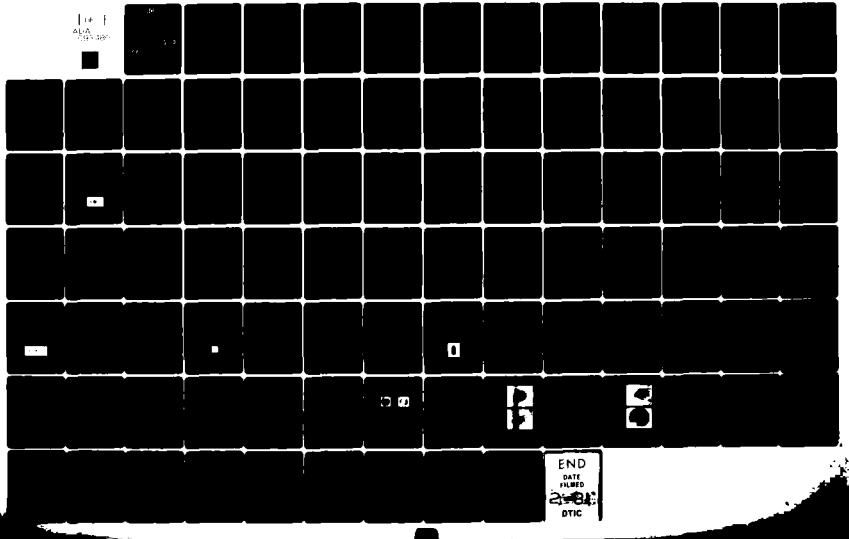

END
DATE FILMED
2-81
DTIC

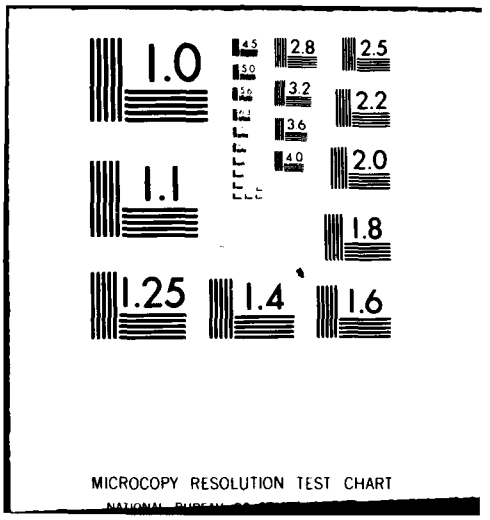
1.0
1.1
1.25
1.4
1.6
1.8
2.0
2.2
2.5
2.8
3.2
3.6
4.0
4.5
5.0
MICROCOPY RESOLUTION TEST CHART

(12) LEVEL III

AD-E430550

AD

AD A093480

CONTRACT REPORT ARBRL-CR-00439

HOLOGRAPHIC IMAGING THROUGH SCATTERING MEDIA

Prepared by

Environmental Research Institute
of Michigan
P. O. Box 8618
Ann Arbor, MI 48107

DTIC
ELECTE
JAN 6 1981
S D
B

October 1980

US ARMY ARMAMENT RESEARCH AND DEVELOPMENT COMMAND
BALLISTIC RESEARCH LABORATORY
ABERDEEN PROVING GROUND, MARYLAND

Destroy this report when it is no longer needed.
Do not return it to the originator.

Secondary distribution of this report by originating or sponsoring activity is prohibited.

Additional copies of this report may be obtained from the National Technical Information Service, U.S. Department of Commerce, Springfield, Virginia 22151.

The findings in this report are not to be construed as an official Department of the Army position, unless so designated by other authorized documents.

The use of trade names or manufacturers' names in this report does not constitute indorsement of any commercial product.

UNCLASSIFIED

SECURITY CLASSIFICATION OF THIS PAGE (When Data Entered)

REPORT DOCUMENTATION PAGE	READ INSTRUCTIONS BEFORE COMPLETING FORM
1. REPORT NUMBER: CONTRACT REPORT ARBRL-CR-00439 / 2. GOVT ACCESSION NO.	3. RECIPIENT'S CATALOG NUMBER
4. TITLE (and Subtitle): HOLOGRAPHIC IMAGING THROUGH SCATTERING MEDIA	5. TYPE OF REPORT & PERIOD COVERED: Final Scientific Report 6/27/79-6/26/80
	6. PERFORMING ORG. REPORT NUMBER: 143400-4-F /
7. AUTHOR(s): Anthony M. Tai and Carl C. Aleksoff, Radar and Optics Division	8. CONTRACT OR GRANT NUMBER(s): DAAK11-79-C-0073
9. PERFORMING ORGANIZATION NAME AND ADDRESS: Environmental Research Institute of Michigan / P.O. Box 8618, Ann Arbor, Michigan 48107	10. PROGRAM ELEMENT, PROJECT, TASK AREA & WORK UNIT NUMBERS: 1L161101A91A
11. CONTROLLING OFFICE NAME AND ADDRESS: US Army Armament Research & Development Command, US Army Ballistic Research Laboratory (DRDAR-BL), Aberdeen Proving Ground, MD 21005	12. REPORT DATE: OCTOBER 1980
	13. NUMBER OF PAGES: 82
14. MONITORING AGENCY NAME AND ADDRESS (if different from Controlling Office)	15. SECURITY CLASS. (of this report): Unclassified
	15a. DECLASSIFICATION/DOWNGRADING SCHEDULE

16. DISTRIBUTION STATEMENT (of this Report)

Approved for public release: distribution unlimited.

17. DISTRIBUTION STATEMENT (of the abstract entered in Block 20, if different from Report)

18. SUPPLEMENTARY NOTES

Dr. Anthony E. Finnerty was the contract monitor for this project.

19. KEY WORDS (Continue on reverse side if necessary and identify by block number)

Scattering media	Grating interferometer
Optical Processing	Interferometric imaging
Holography	Contrast enhancement

20. ABSTRACT (Continue on reverse side if necessary and identify by block number)

Holograhic techniques for imaging through scattering media are reviewed. The concept of an imaging grating interferometer is introduced and its performance in imaging through scattering media is evaluated. The interferometric system is shown to be relatively insensitive to normal vibration and air disturbance. System design and fabrication techniques for the imaging grating interferometer are presented.

DD FORM 1 JAN 73 1473 EDITION OF 1 NOV 65 IS OBSOLETE

UNCLASSIFIED

SECURITY CLASSIFICATION OF THIS PAGE (When Data Entered)

PREFACE

The work reported here was performed in the Electro-Optics Department of the Radar and Optics Division of the Environmental Research Institute of Michigan (ERIM). This work was sponsored by the Army ARRADCOM under Contract DAAK11-79-C-0073.

This report covers work performed between June 27, 1979 and June 26, 1980. The contract monitor was Dr. Anthony Finnerty. The principal investigators were Anthony M. Tai and Carl C. Aleksoff. Major contributors to the effort were Anthony M. Tai, Carl C. Aleksoff, and B. Jin Chang. K. Winick assisted in the fabrication of the grating interferometer.

CONTENTS

Preface..... iii

List of Figures..... vi

1. Introduction..... 1

2. Background..... 3

3. Conventional Holographic Imaging Techniques..... 9

4. Local Reference Beam Holographic Technique..... 17

- 4.1 Dual-Aperture Speckle Interferometer 17
- 4.2 Grating Interferometers 21
- 4.3 Stability Requirements 27
- 4.4 Performance Estimation 34
- 4.5 Recording Material 40
- 4.6 Image Aberrations and Design Parameters 45
- 4.7 Grating Fabrications 56
- 4.8 Widefield Grating Interferometer 62
- 4.9 Experimental Results 65

5. Conclusions and Recommendations..... 76

References..... 79

Distribution List..... 81

LIST OF FIGURES

1. Optical Processing of Coherently Recorded Target Image..... 8
2. Spectral Distribution of Recorded Image..... 8
3. Recording and Reconstruction of Holographic Image Obtained through a Scattering Medium..... 10
4. Recording of an Image Plane Hologram..... 12
5. Optical Processing of Image Plane Hologram..... 12
6. Holographic Recording with Light Source Near the Receiver..... 15
7. Holographic Recording with Light Source Near the Target..... 15
8. Propagation of a Narrow Beam to Avoid Additional Forward Scattering..... 15
9. Dual Aperture Speckle Interferometer..... 18
10. Spectral Distribution of Image Recorded with Dual Aperture Speckle Interferometer..... 20
11. Imaging through a Scattering Medium with a Grating Interferometer..... 22
12. Lateral Shearing of Target Images..... 24
13. Determination of Optimum Grating Frequency..... 25
14a. Coherent Optical Processing of Target Image..... 26
14b. Incoherent Optical Processing of Target Image..... 26
15. Off-Axis Recording of Conventional Hologram..... 30
16. Path Length Variation Due to Displacement of an Optical Component..... 30
17. Recording Geometry of Grating Interferometric System.. 32
18. Path Length Variation Due to Longitudinal Displacement of Target..... 32
19. Dimensions of Grating Interferometer..... 35
20. Estimated System Performances..... 38
21. Characteristics of 649F Plates as a Function of Spatial Frequency..... 41

LIST OF FIGURES
(Continued)

22. Characteristics of 649F Plates as a Function of Exposure..... 43

23. Aberrations Obtained with a Plane Grating Placed Normal to Optical Axis..... 47

24a. Grating Construction Geometry..... 48

24b. Grating Diffraction Geometry..... 48

25a. Correction of Aberration by Tilting Grating..... 50

25b. Aberration Correction for a Converging Beam Diffracted by Two Gratings..... 51

26. An Aberration Free Imaging Grating Interferometer..... 53

27a. Diffraction of a Converging Beam with a Grating Constructed with Plane Waves..... 54

27b. Diffraction of a Converging Beam with a Grating Constructed with Two Diverging Beams..... 55

28a. Fabrication of First Grating..... 57

28b. Diffraction of a Converging Beam by First Grating..... 57

29a. Fabrication of a Second Grating..... 58

29b. Imaging Grating Interferometer..... 58

30. Aberration of an Off Axis Diffraction..... 63

31. Computation of Required Phase Transformation..... 66

32. Fabrication of Wide-Field Diffraction Grating..... 66

33. Evaluation of the System's Imaging Ability..... 67

34. Qualitative Test with Complex Target Using Liquid Crystal Scattering Plate as Scattering Medium..... 69

35. Qualitative Test with 3-D Target Using Diluted Milk as Scattering Medium..... 71

36. Optical Arrangement Utilized for Simulating the Effect of Imaging through a Scattering Medium..... 72

37. Experimental Evaluation of System Performance in Imaging through Scattering Media..... 73

38. Quantitative Test with Two Tone Target..... 74

LIST OF FIGURES
(Continued)

39. Visibility Range as a Function of Visibility Attenuation Coefficient of the Scattering Media..... 77

1
INTRODUCTION

Optical imaging through a scattering atmosphere such as fog and smoke has been an unresolved problem since ancient times. The compass was invented by the Chinese centuries ago to allow their army to advance in heavy fog. The interest in the problem of atmospheric optical transmission is heightened by the development of optical communication, LADAR and laser weapon technologies. A great deal of effort has been geared toward the phase distorting aspect of atmospheric turbulence. However, there have been few viable solutions to the problem of scattering.

Attempts to recreate the target image with the scattered light are generally futile since it is almost an impossible task to determine the time-varying impulse response of a scattering medium. One may however, try to separate the components contributed by the scattered and unscattered light fields and then reconstruct the target image with the unscattered light. Holography has been proposed at various times as a means of separating the scattered and unscattered light fields. The effectiveness of holographic techniques in imaging through fog has been demonstrated quite successfully in the laboratory. However, the conventional holographic techniques that were employed are extremely sensitive to vibration and atmospheric turbulence. This low tolerance renders them impractical in realistic field conditions. In this report, we shall introduce a system that utilizes an imaging grating interferometer to produce a local reference beam hologram with the unscattered light waves. Unlike conventional holographic arrangements, this proposed concept does not require the use of a separate reference beam. This enables the construction of a small and compact system. More importantly, besides providing significant improvement in imaging through a highly scattering atmosphere, the proposed system possesses much higher tolerance to vibration and atmospheric turbulence, distinguishing it as a system feasible for field applications.

In the next section, we define the general problem and establish the rationale for utilizing holographic techniques in imaging through scattering media. The use of the conventional holographic technique is described in Section 3 and its drawbacks in field applications are explained. In Section 4, the grating interferometric imaging system is introduced. Its use in imaging through scattering media is analyzed and its performance is estimated. The optimal design and fabrication technique for the grating system is given. Experimental results with the grating interferometric system for imaging through scattering media are presented.

2
BACKGROUND

When the light field reflected by the target propagates through the scattering atmosphere, it is attenuated by absorption and scattering. In addition, the scattered light creates a time varying background light field. Often, the intensity of this background light is substantially higher than the attenuated signal light. The result is an image of drastically reduced contrast. If the image contrast is below 2%, then the target image would not be recognizable by a human observer[1]. Contrast is defined as

$$\frac{I_{max} - I_{min}}{I_{max} + I_{min}} \times 100\%$$

where I_{max} and I_{min} are the maximum and minimum intensity levels of the image received by the observer. If the target has an intrinsic contrast of 100%, then the intensity of the unscattered light would correspond to

$$I_{unscat} = I_{max} - I_{min}$$

and the intensity of the scattered light would be

$$I_{scat} = I_{min}$$

Contrast can therefore be defined alternatively as

$$\frac{I_{unscat}}{2I_{scat} + I_{unscat}} \times 100\%$$

The SNR of the image obtained through the scattering medium can be defined as

$$SNR = \frac{I_{unscat}}{I_{scat}}$$

$$= \frac{I_{max} - I_{min}}{I_{min}}$$

Thus, the target image would not be recognizable by a human observer if the SNR of the image is lower than 1:25.

The farther the target is from the observer, the larger the volume of scatterers that the reflected light must propagate through. The result is an exponential decrease in image contrast with target range. The image contrast C_I as a function of target range R can be expressed as[2]

$$C_I = C_o \, e^{-\sigma R} \qquad (2\text{-}1)$$

where C_o is the target contrast observed at close range and σ is the visibility attenuation coefficient. The coefficient is dependent on the wavelength of the illuminating light source. The amount of scattering tends to decrease with longer wavelengths.

The average visibility attenuation coefficient for moderately heavy fog under sunlight illumination for example, is about 10 km^{-1}. Thus for a range of 0.35 km, the image contrast of a target with 100 % intrinsic contrast would be

$$C_I = 100 \times 10^{-3.5} = 3\%$$

The target image would be barely recognizable by a human observer. However, the fact that a target is located within the visibility range does not necessarily imply that it will be visible. The 2% minimum contrast criterion applies only to a simple two-tone target. For a complicated continuous-tone target that is imbedded in a background, the image contrast required for human recognition would be substantially higher.

In order to separate the components contributed by the scattered and unscattered light, we must look for a physical characteristic where the two light fields differ. The problem is much simplified if we can make the assumption that the target is stationary within the detection time and the scatterers are in constant motion. The

scatterers are either moving in bulk as they are carried by air current or moving in a random manner due to Brownian motion. First, we examine the difference in velocities between the target and the scatterers. If the target is illuminated with monochromatic light, the light reflected from the stationary target is doppler shifted when it is scattered by the moving scatterers. The bulk type motion would result in a shift in the center frequency of the light and the random motion will cause a broadening of the spectral bandwidth. With the use of a narrow band spectral filter such as a Fabry Perot interferometer, it would be possible to separate out the unscattered light from the doppler shifted scattered light. However, this scheme has some drawbacks. High wind speed can not be relied on and if the wind is blowing traversely across the light path, no doppler shift will be observed. Brownian motion is always present but unless the scattering particles are very small, the particle velocities would not be adequate to produce significant doppler shift. Moreover, even though the particles are in constant motion, their mean velocity is zero. Thus a substantial amount of scattered light would remain within the spectral band of the light source and the separation between the two light fields cannot be complete. Spectral filtering with a Fabry Perot etalon also would not produce an image directly since the system only provides the information on the power of the incoming light field that is within its passband. To produce an image, it would be necessary to look at a small area at a time and build up into a complete image by some form of scanning mechanism.

Alternatively, one can make use of the fact that the moving scatterers create a time-varying light field for the scattered light. With an achromatic grating interferometer[3-4] for example, the lateral position of a point radiator is mapped into the spatial frequency of a sinusoidal fringe pattern. The moving scatterers would therefore create fringe patterns of varying frequencies. If the moving scatterers are constantly moving to new, never occupied

positions in the field of view during the integration time T, the time-averaged contrast of the fringes formed by the scattered light would only be 1/T of that produced by the stationary point target.

However, this would approximately be true only if the number of scatterers is much smaller than the space bandwidth in the field of view of the imaging system. In most practical applications (e.g., imaging through fog), the sizes of the scatterers and the spacings between them are both beyond the resolution limit of the imaging system. For an incoherently illuminated target, the modulus-squared of the point spreads functions will merge to form a continuous intensity pattern. Thus, even though the scatterers are in constant motion, the intensity distribution of the scattered light field would appear stationary to the imaging system. The SNR cannot be improved by time-averaging if the target is incoherently illuminated.

In order to separate the scattered and unscattered light, it would be necessary to illuminate the target by coherent light. If the target is imaged through a scattering media, the unscattered light would form a speckled image[5].

$$|f(x, y) * h(x, y)|^2$$

where $f(x, y)$ is the target function and $h(x, y)$ is the impulse response of the imaging system and * denotes convolution operation. On the other hand, the scattered light produces a time-varying speckle pattern which in time averages out into a uniform bias. Thus, by recording the image over a sufficiently long integration time, we would obtain

$$T_A(x, y) = B^2 + A^2|f(x, y) * h(x, y)|^2 \qquad (2\text{-}2)$$

where B^2 and A^2 are the intensities of the scattered and unscattered light. Inserting the transparency with an amplitude transmittance of $T_A(x, y)$ into the optical processor as shown in Figure 1, we would have, at the spatial frequency plane[5],

$$\mathcal{F}[T_A(x, y)] = B^2\delta + A^2[F(p, q)\, H(p, q) * \bar{F}(-p, -q)\, \bar{H}(-p, -q)] \quad (2\text{-}3)$$

where the top bars denote conjugates and $\mathcal{F}(\cdot)$ is the Fourier transform,

$$\mathcal{F}[T_A(x, y)] = \iint_{-\infty-\infty}^{\infty\ \infty} T_A(x, y)\, e^{-i(px+qy)}\, dx\, dy \quad (2\text{-}4)$$

For a diffuse object $|F(p, q)| \approx$ constant and the spectral distribution of the target image would simply equal to $|H(p,q)*\bar{H}(p,q)|$ as illustrated in Figure 2. Since the spectrum of the uniform bias concentrates at the origin of the frequency plane, it can be filtered out with a dc stop. At the output, we would obtain a target image of improved contrast. However the improvement achieved with this simple technique is limited. First of all, the Fourier transform is performed over a finite aperture. Thus, instead of a delta function, we would obtain for the bias term a diffraction pattern corresponding to the Fourier transform of the input aperture. Since $B^2 >> A^2$, the sidelobes of the dc term could contribute significantly to the filter image. Secondly, the energy of the image spectrum also centers around the origin. In performing the high pass filtering, a substantial amount of signal energy would be lost. To make the matter worse, system noise such as film grain noise is highest at low frequencies[6]. The high noise level together with the inefficient filtering process severely limit the amount of contrast improvement attainable.

To produce a much higher degree of contrast improvement, an effective approach is to shift the signal image spectrum away from the dc term to a region where the system noise is lower. This would also allow the entire image spectrum to pass through the filter. To produce the necessary carrier frequency, various holographic techniques can be utilized.

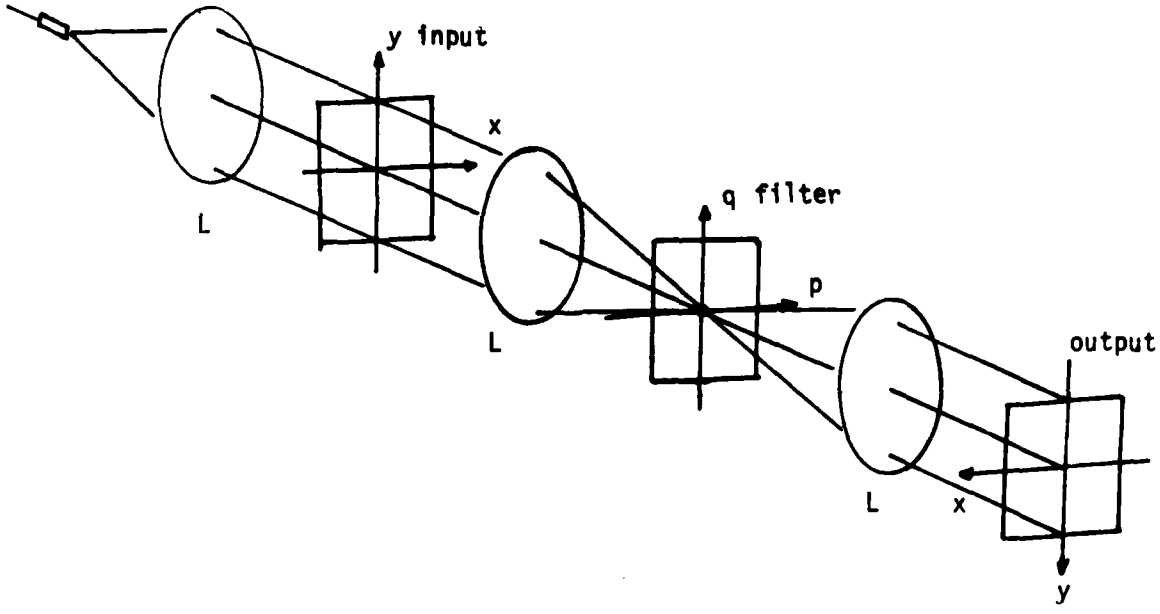

FIGURE 1. OPTICAL PROCESSING OF COHERENTLY RECORDED TARGET IMAGE

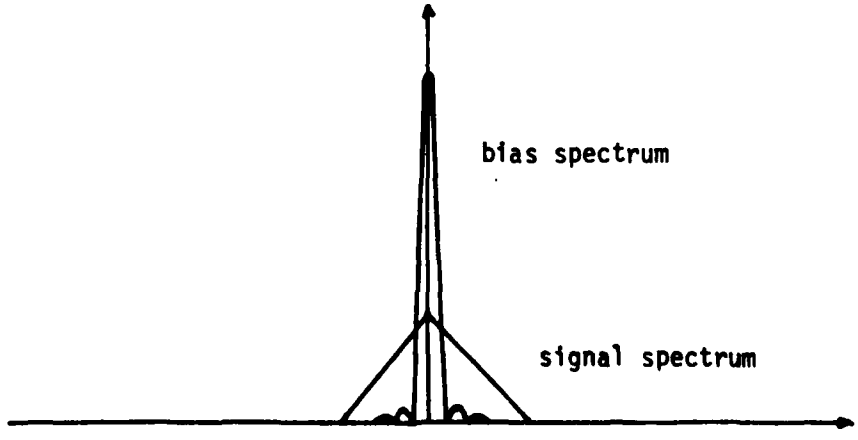

FIGURE 2. SPECTRAL DISTRIBUTION OF RECORDED IMAGE

3
CONVENTIONAL HOLOGRAPHIC IMAGING TECHNIQUES

If the incoming light field is made to interfere with a stationary coherent light beam (reference beam), the unscattered portion of the received light field will produce a stationary fringe pattern while the scattered light will produce time-varying patterns. Recording these interference patterns with an integrating detector such a photographic film or CCD detector arrays, the time-varying patterns will in time be averaged into a uniform bias. Except for this added background bias, the time-averaged interference pattern would be identical to that produced by the object light field without the presence of the scattering media.

With the addition of a reference beam and the recording of the interference pattern as illustrated in Figure 3, a hologram of the target is being recorded through the scattering medium.[7] The light intensity distribution at the recording plane can be written as[5]

$$I(x, y) = B^2 + \left| \frac{A_e^{ikR}}{i\lambda R} \int_{-\infty}^{\infty}\int_{-\infty}^{\infty} f(\alpha, \beta) e^{\frac{ik}{2R}[(x-\alpha)^2 + (y-\beta)^2]} d\alpha\, d\beta + C\, e^{-ik \sin \theta x} \right|^2 \qquad (3\text{-}1)$$

where $f(\alpha, \beta)$ is the light distribution at the target plane and R is the distance between the target and the recording plane.

After recording this light field linearly, the developed hologram is then illuminated by an off axis coherent light beam. The field of the unscattered light will be reconstructed to product the light field of the unscattered light. By imaging this light field (or by simply looking into the reconstructed beam), the target image can be obtained with much of the background bias eliminated. However, with the cases of interest, $B^2 >> A^2$ and we must maximize the signal level to produce a satisfactory image. Since the point radiators on

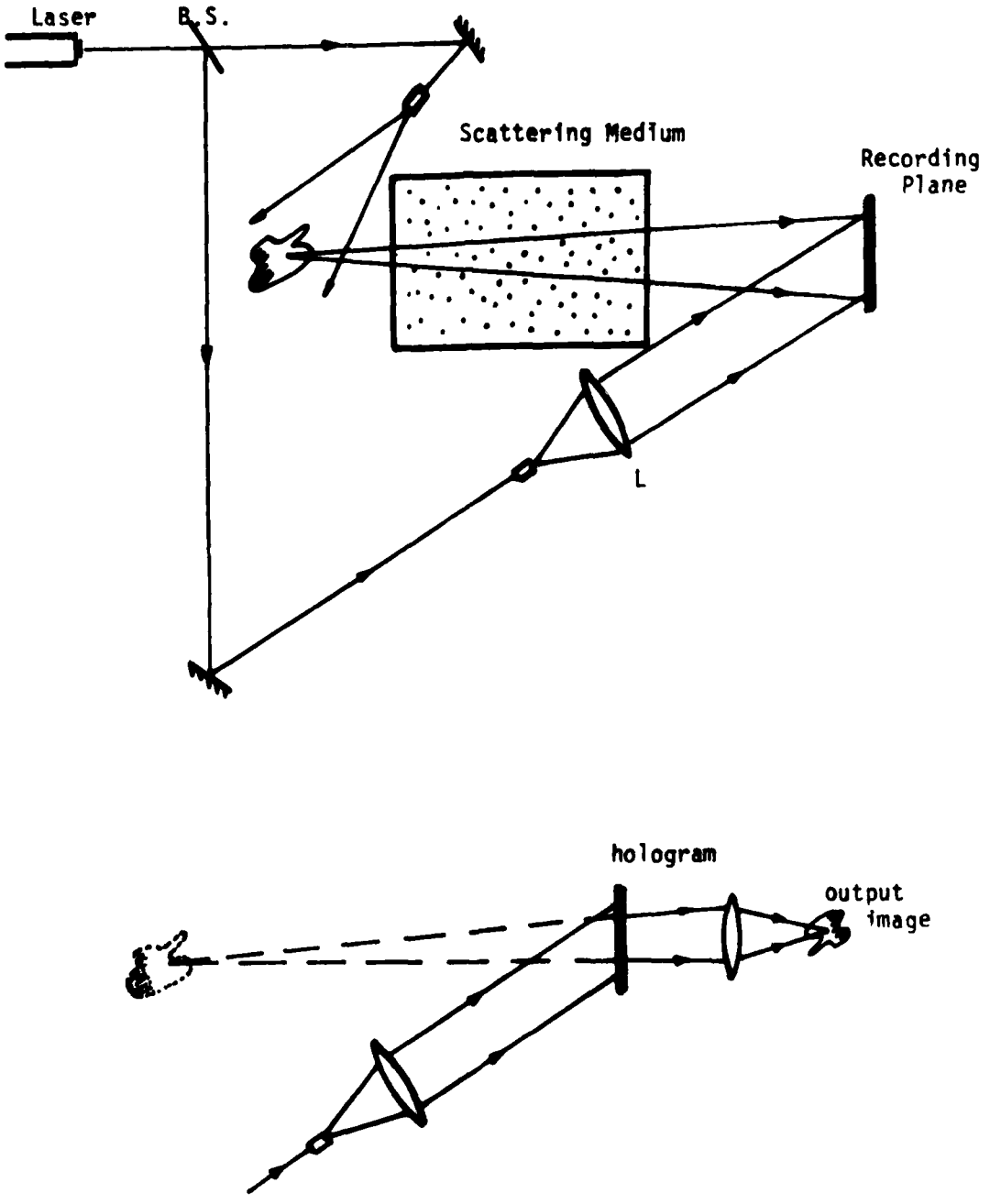

FIGURE 3. RECORDING AND RECONSTRUCTION OF HOLOGRAPHIC IMAGE OBTAINED THROUGH A SCATTERING MEDIUM

the illuminated target are all concentrated at a lateral plane while the scatterers are distributed over a large volume, the signal level can be maximized by imaging the target on the recording plane and construct an image plane hologram as illustrated in Figure 4. The light intensity distribution at the recording can then be written as

$$B^2 + \left| A\,|f(x, y) * h(x, y)|\, e^{i\phi(x,y)} + C\, e^{-ik \sin \theta x} \right|^2 \qquad (3\text{-}2)$$

where A and B are the amplitudes of the unscattered and scattered light, C is the amplitude of the reference beam, $f(x, y) * h(x, y)$ is the amplitude and $\phi(x, y)$ is the phase distributions of the image field. For maximum diffraction efficiency, the amplitude of the reference beam should be made to be the same as the unscattered light. That is, $A = C$. And since $B^2 \gg A^2$ for the cases of interest, the light intensity distribution at the image plane can be approximated by

$$I(x, y) \tilde{=} 1 + 2\left(\frac{A}{B}\right)^2 f(x, y) * h(x, y)$$

$$\cdot \cos [k \sin \theta x + \phi(x, y)] \qquad (3\text{-}3)$$

Recording the intensity pattern linearly on a photographic plate and then illuminating the developed transparency with the reference beam, the unscattered object wave would be reconstructed. The reconstructed wavefront can then be imaged onto the output plane with a relay lens as shown in Figure 5. We would once again obtain the target image with a substantially improved contrast.

Such a technique has been demonstrated in the laboratory successfully. However, its effectiveness is severely limited when applied in actual field conditions. First of all, to image a target a distance away, an equivalent path length must be provided for the

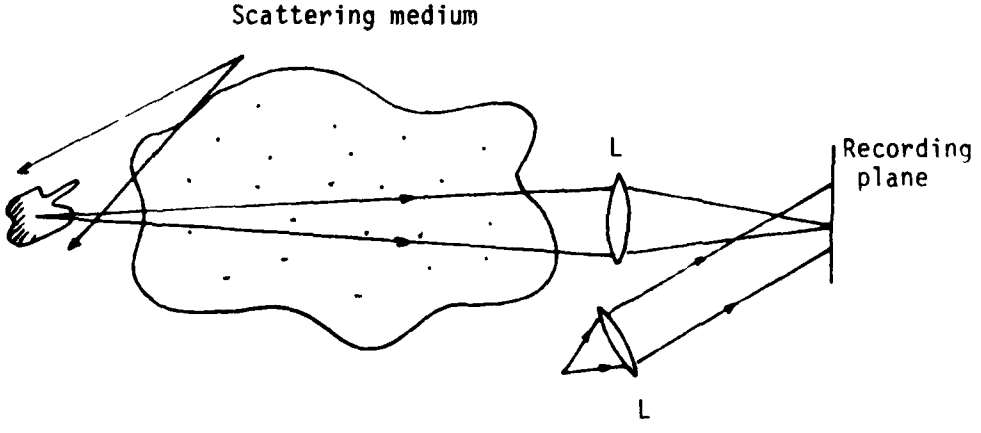

FIGURE 4. RECORDING OF A IMAGE PLANE HOLOGRAM

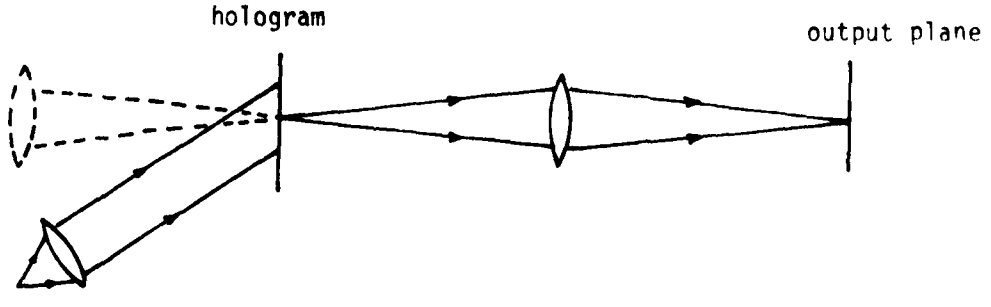

FIGURE 5. OPTICAL PROCESSING OF IMAGE PLANE HOLOGRAM

reference beam. This would require the prior knowledge of the target range to within the coherence length of the light source. Since the target is obscured, such a precise knowledge of the target range generally cannot be assumed. Secondly, the ideal optical arrangement depicted in Figure 4, is not a realistic simulation of what could be implemented in the field. For example, if the light source is located near the receiver as shown in Figure 6, there would be severe backscattering from the illuminating beam. Even if we assume that this backscattering can be eliminated by pulse gating techniques, the illuminating beam still has to propagate through the scattering atmosphere to the target. Only the portion of the illuminating light that travels to and back from the target unscattered will be able to produce stationary fringes. The light intensity distribution obtained with such an arrangement can be approximated as

$$I(x, y) = 1 + 2\left(\frac{A}{B^2}\right)^2 \left| f(x, y) * h(x, y) \right|$$

$$\cos [k \sin \theta x + \phi(x, y)] \qquad (3\text{-}4)$$

On the other hand, if the light source is placed near the target as illustrated in Figure 7, the reference beam would be scattered as it travels to the receiver, creating additional forward scattered light. Under optimum beam ratio, the light intensity distribution would be

$$I(x, y) = 1 + \left(\frac{A}{B}\right)^2 \left| f(x, y) * h(x, y) \right|$$

$$\cos [K \sin \theta x + \phi(x, y)] \qquad (3\text{-}5)$$

It can be shown that the SNR of the reconstructed image is proportional to M^2 where M is the modulation depth of the recording. Assuming that the recording is linear, then the ratio of the SNR

between the ideal condition of Figure 4 and the more realistic conditions of Figure 6 where the light source is placed near the receiver and Figure 7 where the light source is placed near the target would be

$$\left[2\left(\frac{A}{B}\right)^2\right]^2 : \left[2\left(\frac{A}{B^2}\right)^2\right]^2 : \left[\left(\frac{A}{B}\right)^2\right]^2$$

For example, if $A^2/B^2 = 1/100$, then the ratio would be

$$1 : \frac{1}{100} : \frac{1}{4}$$

Thus, a much better SNR can be obtained with the light source placed near the target instead of the receiver. However, the SNR would still be a factor of 4 lower than the ideal condition where the light beams can illuminate both the target and the receiver without first being scattered. It should be noted here that the ideal condition can be achieved by propagating a narrow reference beam to the receiver and then expanding the beam near the receiver with a spatial filter as shown in Figure 8. The narrow beam will produce very little additional scattered light and the spatial filter will allow only the unscattered light to pass through. However, the receiver would also be obscured by the scattering atmosphere and it would be difficult to aim a narrow beam precisely at the receiving optics in actual field conditions. Such an arrangement would be restricted to applications where the optics can be fixed in prealigned positions.

The most important drawback of the conventional holographic technique however, is its extreme sensitivity to phase shift between the interfering beams. Such a phase shift could be due to displacements between the various components or changes in the refractive index of the medium in the light path. In a laboratory, all the components including the target, receiving optics and light source can be mounted rigidly on an isolated optical bench. In a controlled laboratory environment, the refractive index of the air within the light

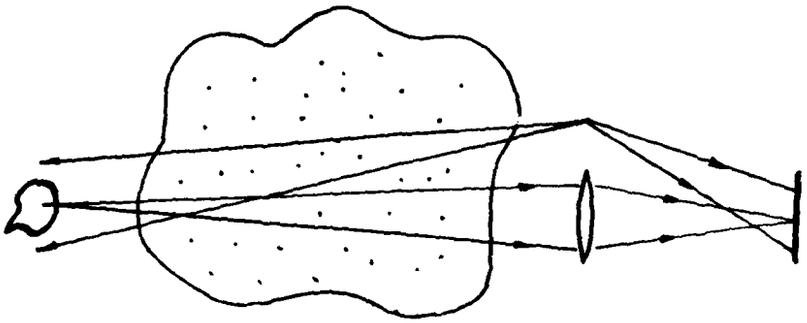

FIGURE 6. HOLOGRAPHIC RECORDING WITH LIGHT SOURCE NEAR THE RECEIVER

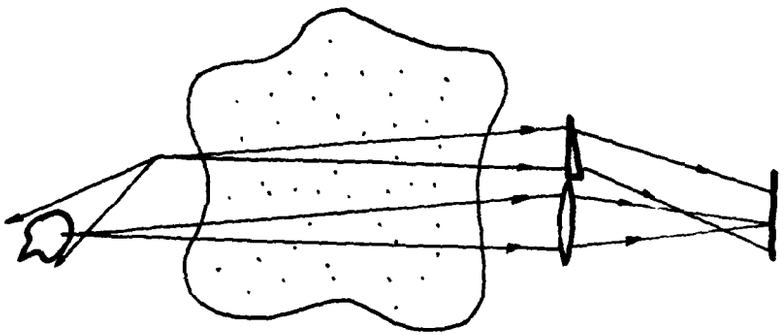

FIGURE 7. HOLOGRAPHIC RECORDING WITH LIGHT SOURCE NEAR THE TARGET

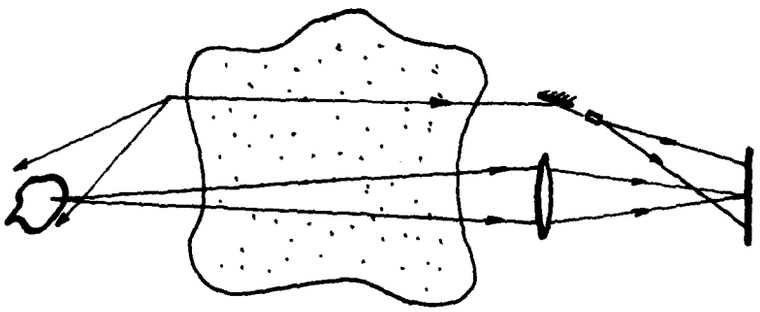

FIGURE 8. PROPAGATION OF A NARROW BEAM TO AVOID ADDITIONAL FORWARD SCATTERING

paths can also be maintained at a very constant level. However, in real world application of the holographic system, the various components controlling the interfering beams would be spaced widely apart with a dynamic air mass between them. These components would vibrate independently and it is likely that the relative positions of the components would change more than a wavelength during the integration time. Moreover, with the interfering light beams traveling through different light paths, atmospheric effect such as turbulence could easily change the phase difference between the beams by a wavelength or more. Thus even though the conventional holographic technique has been applied successfully in the laboratory, it cannot be implemented effectively outside the laboratory under actual field conditions. The stability requirement for the conventional holographic technique will be discussed in better details in a later section.

4
LOCAL REFERENCE BEAM HOLOGRAPHIC TECHNIQUE

The basic concept employed by the holographic technique is to create sinusoidal modulation for unscattered light. The modulated signal is then separated from the dc bias created by the scattered light using high pass or band pass spatial filtering. The need for a reference beam however, has limited their usefulness in practical applications. As we shall show, the same basic concept can be implemented without the use of a separate reference beam. We can produce the sinusoidal modulation of the unscattered light by interfering the image light field with itself.

4.1 DUAL-APERTURE SPECKLE INTERFEROMETER

Let us first consider the simple system illustrated in Figure 9. It consists of an imaging lens with two apertures of diameter d and separation D. For a target f(x, y), we would have at the image plane, a light distribution of

$$I(x, y) = \left|f(x, y) * h(x, y)\right|^2 \left\{1 + \cos\left[\frac{2\pi Dx}{\lambda} + \phi(x, y)\right]\right\} \quad (4\text{-}1)$$

where h(x, y) is the impulse response of the imaging system.

We have therefore obtained a sinusoidally modulated target image whose spatial frequency is proportional to the separation distance D between the apertures[8]. If a scattering medium is placed between the target and imaging lens, the light scattered by the medium will lose its spatial coherence and the scattered light fields will add by their intensities while the unscattered light fields interfere with each other. The resulting intensity distribution can be written as

$$B^2 + A^2 \left|f(x, y) * h(x, y)\right|^2 \left\{1 + \cos\left[\left(\frac{2\pi Dx}{\lambda}\right) + \phi(x, y)\right]\right\} \quad (4\text{-}2)$$

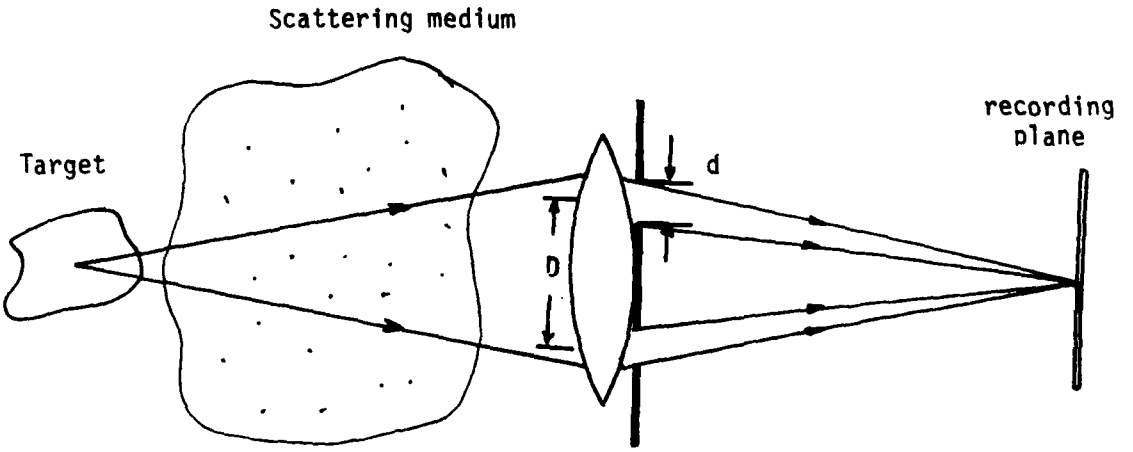

FIGURE 9. DUAL APERTURE SPECKLE INTERFEROMETER

where B^2 and A^2 are the intensity of the scattered and unscattered light at the image plane respectively. Thus, aside from a decrease in fringe visibility, the light pattern is essentially unchanged by the scattering. If this light pattern is recorded linearly on a photographic film, the modulated target image can be extracted from the background bias by simple bandpass filtering using an optical processor. To optimize SNR, the filter bandwidth should be equivalent to the signal bandwidth. The bandwidth of the modulated term is equal to the width of

$$\mathcal{F}|f(x, y) * h(x, y)|^2 = |F(p, q)\, H(p, q)$$

$$* \overline{F}(-p, -q)\, \overline{H}(-p, -q)|$$

Once again for a diffused target we may assume that $|F(p, q)| \approx$ constant and the image bandwidth would be determined by

$$|H(p, q) * \overline{H}(-p, -q)|$$

Thus, the image bandwidth would be equal to $2d/\lambda\ell$, the width of the incoherent transfer function. Since the locations of the sidebands are determined by the modulation frequency $\cos(2\pi Dx/\lambda\ell)$, the minimum separation between the apertures must be $D = 2d$ as illustrated in Figure 10, in order for the signal to be separated completely from the zero order term. However, to achieve satisfactory SNR, we should make $D > 2d$. First of all, the dc bias term for a low contrast input is much larger than the modulated signal. Unless the image spectrum is translated far enough away from the dc term (by increasing D), the zero order sidelobes would contribute significantly to the filtered image. Moreover, system noise such as grain noise drops sharply as we move away from the zero order. Better SNR can therefore be obtained with the use of higher modulation frequencies.

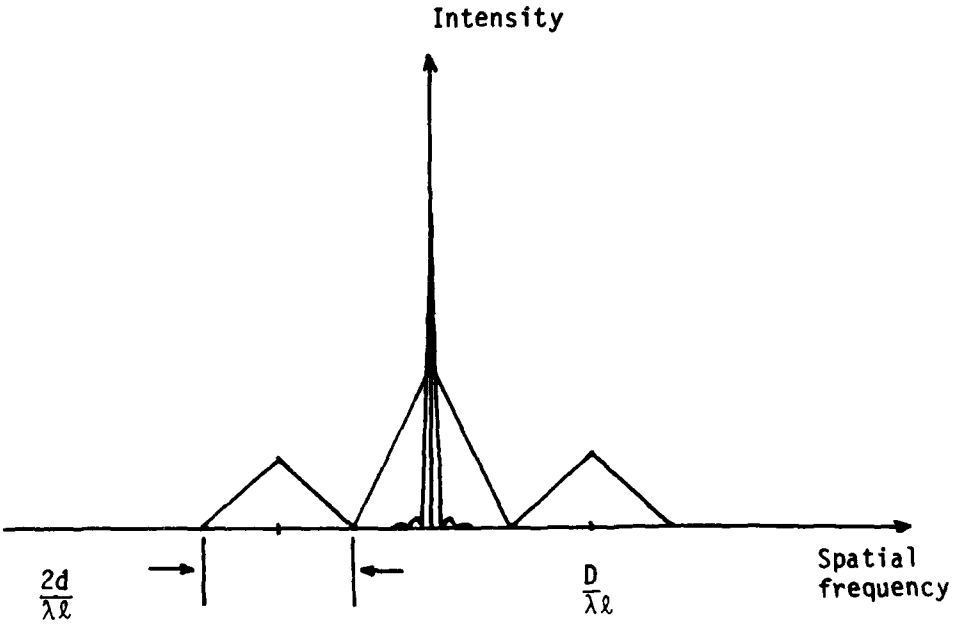

FIGURE 10. SPECTRAL DISTRIBUTION OF IMAGE RECORDED WITH DUAL APERTURE SPECKLE INTERFEROMETER

While D should be maximized for optimum SNR, d should be minimized. The system noise (e.g., grain noise) within the filter bandwidth may be approximated to be white. The amount of noise power transmitted through the filter would then be proportional to the filter bandwidth. Since the filter bandwidth is designed to be equivalent to the image bandwidth, the SNR is maximized by minimizing d. However, we cannot arbitrarily increase D and decrease d. With the system shown in Figure 9, the separation D is limited by the lens aperture. The maximum separation would be D = A - d where A is the diameter of the lens. Nevertheless, we shall later show that this limitation can be eliminated with the use of a grating interferometer. Decreasing d on the other hand would simultaneously reduce the resolution and efficiency of the system. With most applications, the resolution requirements for achieving identification are not very high and we find that generally, the lost in efficiency is the more detrimental effect.

The use of very small apertures may require an overly long exposure to compensate for the low light gathering efficiency of the system. The minimum aperture size is thus determined by the longest exposure time allowable by the particular application.

4.2 GRATING INTERFEROMETERS

The modulation frequency achievable with the dual-aperture system is limited by the numerical aperture of the lens. To overcome this limitation, an imaging system utilizing a grating interferometer can be used. One possible arrangement is shown in Figure 11. The first grating separates the input light field into two parts and the second grating recombines them. The gratings are volume gratings of the same spatial frequency constructed with dichromated gelatin. The first grating is made to have a diffraction efficiency of 50% while the second grating approaches 100%. Thus aside from absorption, nearly all of the input light energy is directed to the output plane.

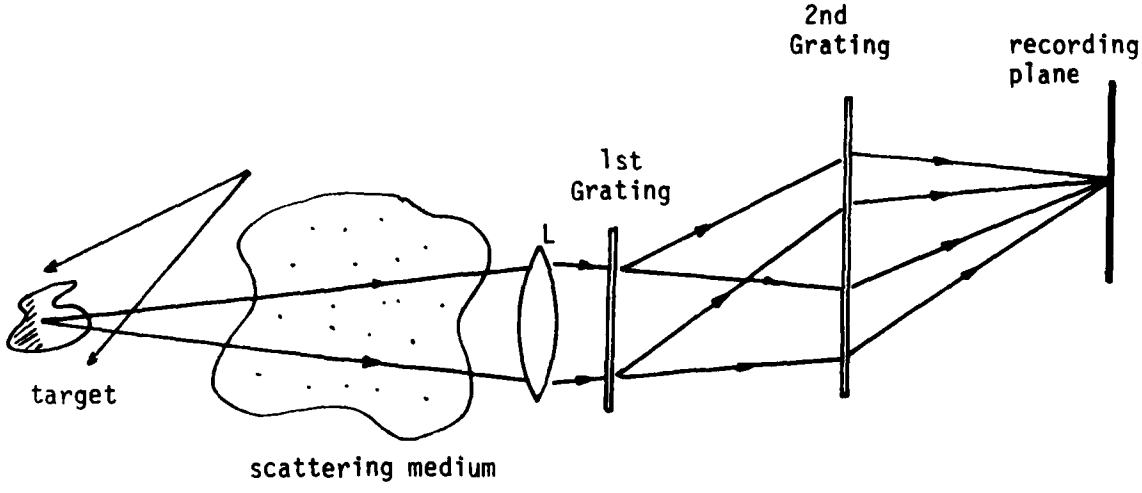

FIGURE 11. IMAGING A SCATTERING MEDIUM WITH A GRATING INTERFEROMETER

It can be shown that at plane $z = 0$, stationary fringes with spatial frequency identical to that of the gratings are formed regardless of the phase variation of the input light field[3-4]. Thus stationary fringes will be formed by both the unscattered light and the spatially incoherent scattered light. In order to allow only the unscattered light to form stationary fringes, a lateral shear of the image field is produced by moving the output plane to $z = \Delta z$ as shown in Figure 12. The output intensity distribution can be approximated to be

$$B^2 + A^2 \left| f(x, y) * h(x, y) \right|^2$$

$$\left\{ [1 + \cos (2\pi G_o x + \phi(x, y)] \right\} \qquad (4\text{-}3)$$

where B^2 and A^2 are the intensities of the scattered and unscattered light at the image plane respectively. The light pattern is thus similar to that obtained with the dual-aperture system except that the modulation frequency is now determined by the grating frequency G_o. The optimum choice of G_o is dependent on the characteristic of the recording material utilized with the system. For many materials such as photographic film, the amount of scattered noise decreases almost exponentially with spatial frequency. On the other hand, the MTF of the recording material also decreases with spatial frequency. The fringe contrast would be reduced if the modulation frequency is too high. An optimum modulation frequency therefore exist as illustrated in Figure 13. The grating frequency G_o should be chosen such that it matches the characteristics of the recording material.

To process the recorded transparency to extract the modulated target image from the background bias, a coherent optical processor as shown in Figure 14(a) can be used. The Fourier transformation of the input transmittance function is performed by the converging

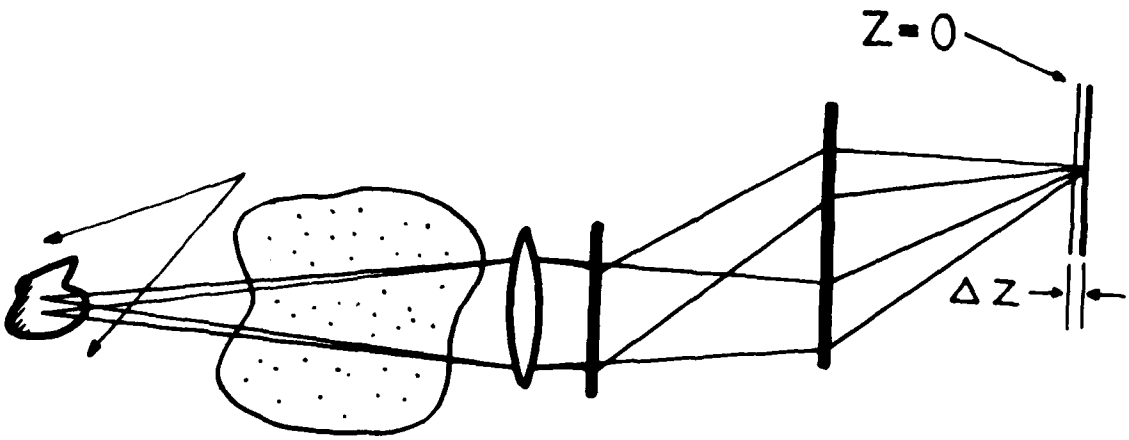

FIGURE 12. LATERAL SHEARING OF TARGET IMAGES

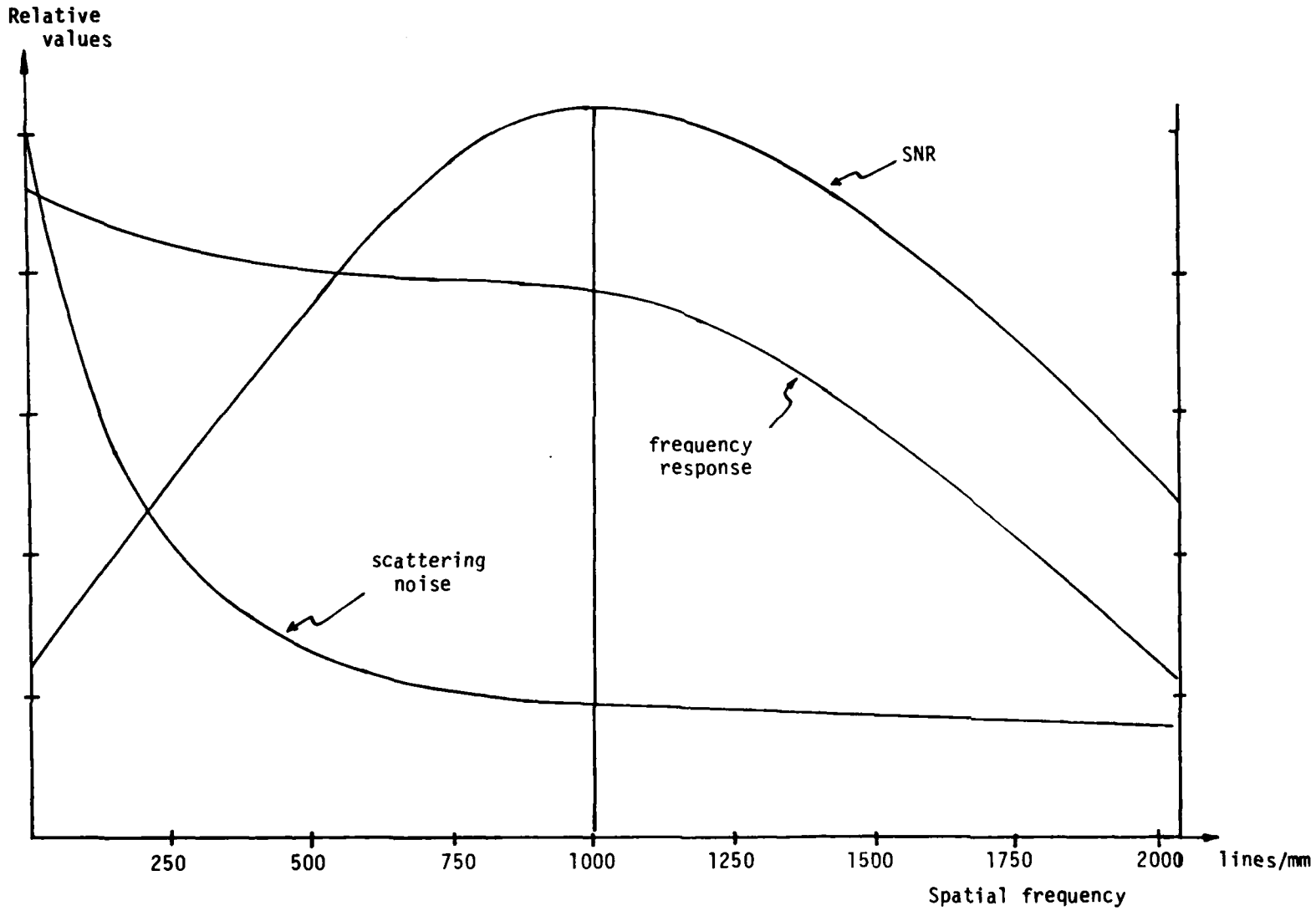

FIGURE 13. DETERMINATION OF OPTIMUM GRATING FREQUENCY

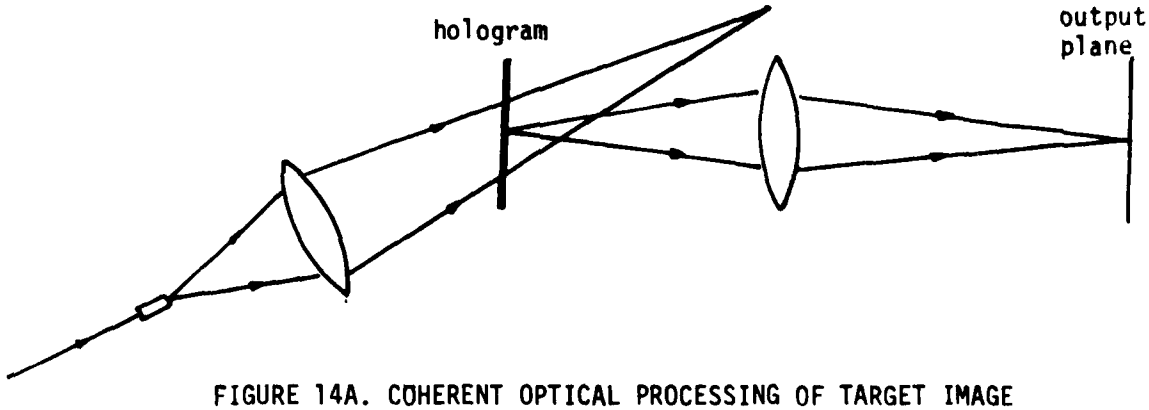

FIGURE 14A. COHERENT OPTICAL PROCESSING OF TARGET IMAGE

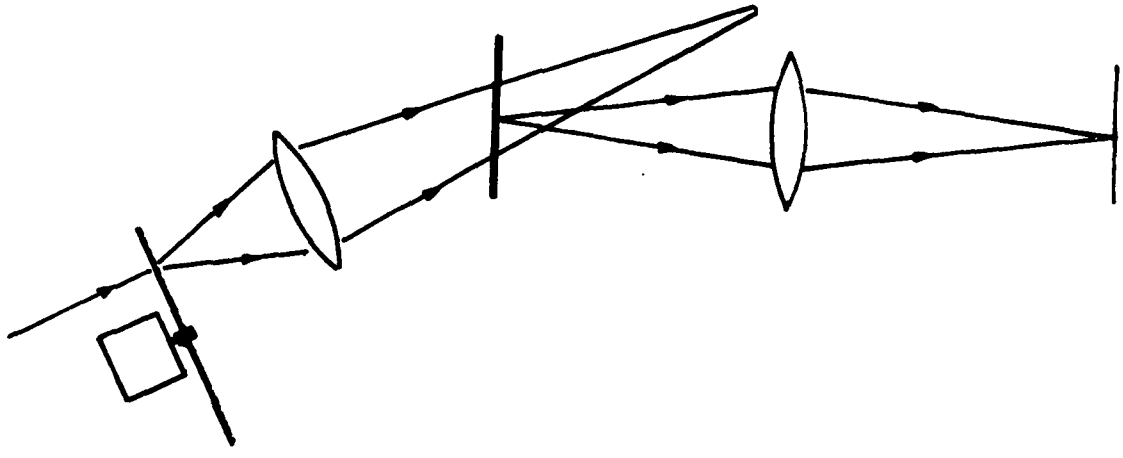

FIGURE 14B. INCOHERENT OPTICAL PROCESSING OF TARGET IMAGE

beam. The lens aperture is placed in the spatial frequency plane at a position that corresponds to the carrier frequency of the modulated signal. The lens aperture would act as the bandpass filter and the aperture size is set according to the bandwidth of the signal spectrum.

The input transparency is imaged onto the output plane by the processing lens. Since only the modulated area of the input will diffract light to the lens aperture, the modulated target image will be separated from the zero order term to produce an output image with significantly improved contrast.

The recording is essentially a local reference beam image plane hologram and as with other types of image plane holograms, incoherent light can be used to reconstruct the holographic image[7]. One versatile approach is to make use of spatially incoherent light. A light source with varying degrees of spatial coherence can be obtained by focusing a coherent light beam on a rotating ground glass diffuser. To decrease the spatial coherence, one may simply increase the spot size of the focused beam. We find that by directly illuminating the rotating diffuser with a laser beam as shown in Figure 14(b), a substantial reduction of the coherent noise can be achieved without overly affecting the SNR of the processed image. Alternatively, one can make use of a light source with an appropriate spectral bandwidth to create similar effects. A high power LED would be a very good candidate due to its small size and modest cost.

4.3 STABILITY REQUIREMENTS

The major advantage offered by the local reference beam holographic technique is its relatively insensitivity to vibration and atmospheric turbulence. First, let us examine the stability requirements for recording a conventional hologram.

In Figure 15, we illustrate the basic geometry for recording a hologram with an off-axis reference beam. The light field impinging on the recording plane can be written as

$$E(x, y) = |E_R(x, y)| e^{i\left[\omega\left(t - \frac{L_R}{V_1}\right) + \phi_R(x,y)\right]} + |E_0(x, y)| e^{i\left[\omega\left(t - \frac{L_0}{V_2}\right) + \phi_0(x,y)\right]} \quad (4\text{-}4)$$

where V_1 and V_2 are the velocities of propagation through the two optical paths ($V = c/n$ where c is the velocity of light in free space and n is the refractive index). Recording the light intensity on a photographic plate, the resulting transparency would have a transmittance of

$$T_A(x, y) = |E_R(x, y)|^2 + |E_0(x, y)|^2 + 2|E_R(x, y)| \; |E_0(x, y)| \cos\left[\left(\phi_R(x, y) - \phi_0(x, y)\right) + \omega\left(\frac{L_R}{V_1} - \frac{L_0}{V_2}\right)\right] \quad (4\text{-}5)$$

In order to record the fringe pattern with the highest possible contrast, the fringe pattern should remain stationary during the exposure. Any changes in the phase of the sinusoidal interference pattern will have a smearing effect on the recording.

Let us first assume that the recording material is rigidly mounted and the largest permissible fringe movement is one-tenth of a period. Any changes in L_R, L_0, V_1 or V_2 will produce a shift in the interference pattern. From Eq. 4-5 we can see that to satisfy the stability requirement, it would be necessary that

$$\Delta\left[\omega\left(\frac{L_R}{V_1} - \frac{L_o}{V_2}\right)\right] \leq \frac{2\pi}{10} = \frac{\pi}{5} \tag{4-6}$$

If the refractive indices in the two light paths are both equal to 1, we obtain

$$\Delta \frac{\omega}{c} (L_R - L_o) \leq \frac{\pi}{5} \tag{4-7}$$

Illuminating with a laser source that emits at 0.6328 μm, we have

$$\Delta(L_R - L_o) \leq 63.28 \text{ nm}$$

That is, the change in the path difference during exposure must be less than 63.28 nm.

The change in the path difference can be caused by movement (vibration) of the target or the beam steering optics. To avoid a change in path difference of more than 63.28 nm, the components must not be allowed to move for more than a fraction of that amount. For example, if the illuminating beam is reflected off a component at an angle θ as illustrated in Figure 16, a longitudinal displacement of d for the component will produce a change in path length of

$$\Delta L = \frac{d}{\cos \theta} (1 + \cos 2\theta) \tag{4-8}$$

For $\theta = 15^{\circ}$, the maximum permissible displacement for the component would only be 32.76 nm.

We now assume that the components in the optical arrangement are stationary during the exposure but the refractive indices vary. Since $(L_R - L_o) <$ coherent length, we may approximate $L_R = L_o = L$ and express Eq. (4-6) as

$$\Delta\left[\omega L\left(\frac{1}{V_1} - \frac{1}{V_2}\right)\right] = \Delta\left[\frac{\omega L}{c}(n_1 - n_2)\right] \leq \frac{\pi}{5} \tag{4-9}$$

For L = 1 km, the changes in the refractive indices must be less than

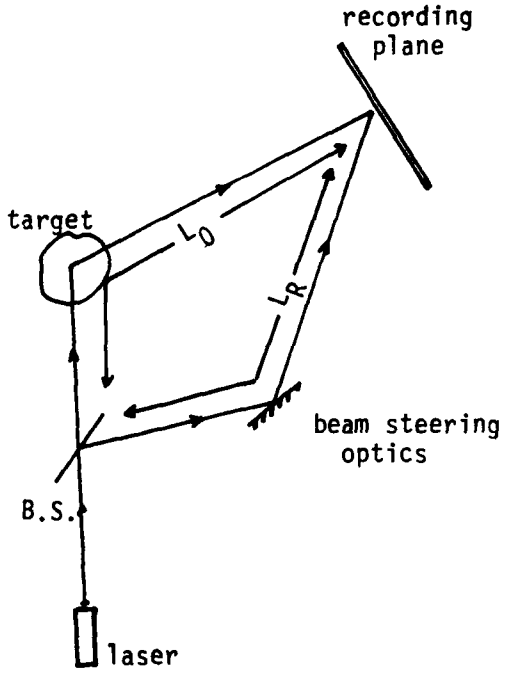

FIGURE 15. OFF-AXIS RECORDING OF CONVENTIONAL HOLOGRAM

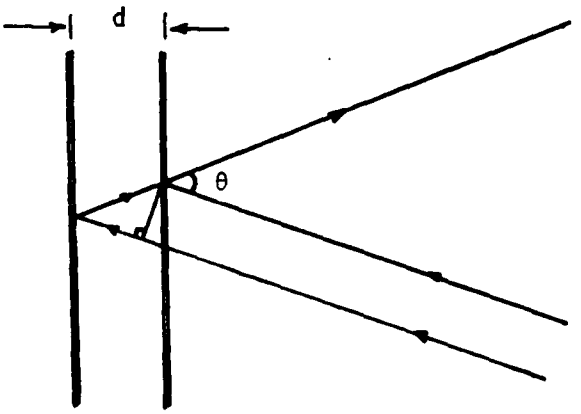

FIGURE 16. PATH LENGTH VARIATION DUE TO DISPLACEMENT OF AN OPTICAL COMPONENT

$$\Delta(n_1 - n_2) \leq 3.98 \times 10^{-10}$$

Inside a controlled laboratory requirement it is possible to meet these stringent requirements. However, under actual field conditions, it is unlikely that these requirements can be satisfied. Components are mounted independently and widely apart. Their relative displacement due to normal vibration can easily exceed the acceptable limit. Moreover, these components are separated by a dynamic air mass. The refractive indices of the air mass changes constantly and with a variation much greater than 3.98×10^{-10}. We can therefore conclude that the conventional hologram would not be practical in actual field conditions.

To examine the stability requirement for recording a local reference beam hologram with our grating interferometric imaging system, we shall first assume that the recording material is rigidly mounted and free of vibrations. Once again, to ensure that the fringes would not move for more than one-tenth of a period, it is necessary that

$$\Delta(L_R - L_O) \leq 63.28 \text{ nm}$$

With the grating interferometer however, the two interfering light beams travel through a nearly identical light path. For example, with the system illustrated in Figure 17, a lateral shear of Δx between the two interfering images would correspond to a shear of $S = 1000\ \Delta x$ at the target plane 1 km away. If the target is under the illumination of a collimated beam incident at an angle θ, the light paths of two interfering light waves may be illustrated as in Figure 18. Displacing the target longitudinally by a distance d will produce a change in path difference of

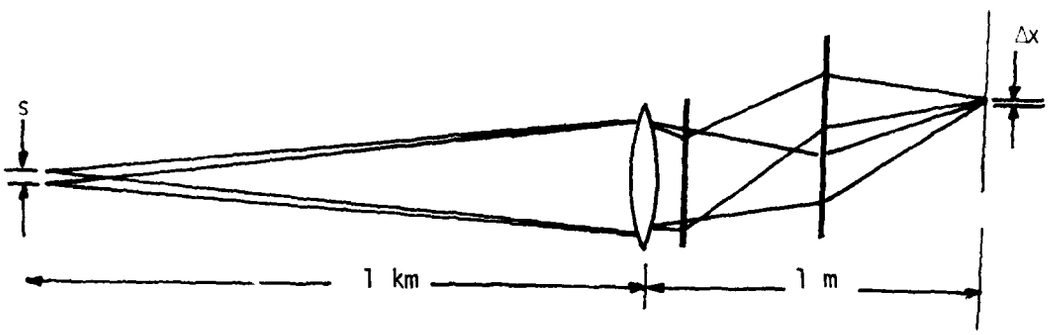

FIGURE 17. RECORDING GEOMETRY OF GRATING INTERFEROMETRIC SYSTEM

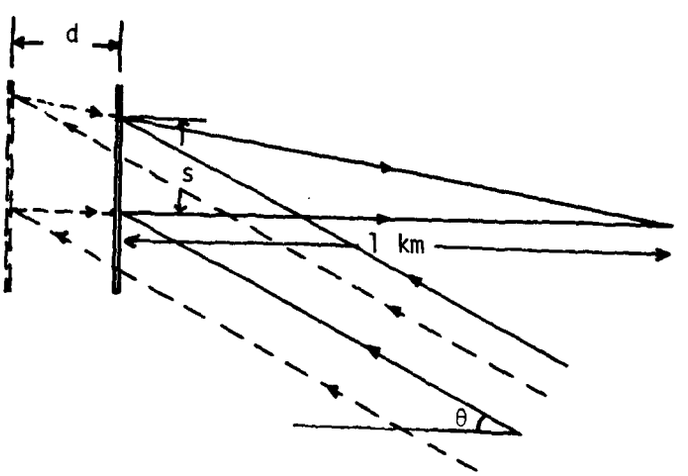

FIGURE 18. PATH LENGTH VARIATION DUE TO LONGITUDINAL DISPLACEMENT OF TARGET

$$\Delta(L_R - L_o) = d \left[\frac{S}{R} \sin \theta + \frac{1}{\cos\left(\tan^{-1} \frac{S}{R}\right)} - 1 \right] \qquad (4\text{-}10)$$

For example, if S = 100 mm (or Δx = 0.1 mm) and R = 1 km, in order to satisfy the condition that $\Delta(L_R - L_o) \leq 63.28$ nm, the longitudinal motion of the target must be limited to

$$d \leq 2.4 \text{ mm}$$

If the target moves laterally, the main effect is to produce a corresponding lateral shift of the fringes. However, due to the demagnification factor of 1000, the amount of permissible lateral motion would be $d \leq 0.1$ mm for a 1000 lines/mm modulation frequency.

The use of the local reference beam holographic technique with a grating interferometer has eliminated the need of separate beam steering optics for the two interfering light beams. And as we have shown, it also relaxes substantially the stability requirement for the target to a level that can be satisfied in the field.

We had assumed that the recording material is free of any vibration. The permissible amount of motion for the recording material (and the receiving optics) is the same for the conventional and local reference beam techniques, that is, one-tenth of a period of 0.1 μm. Fortunately, one has full control of the receiving side of the system and motions within the receiver can be easily reduced to the acceptable level by rigid mounting and vibration isolation.

The changes in the refractive index of the air mass in the light path have a severe effect on the conventional holographic technique because the interfering light beams have to travel through very different light paths. With the local reference beam technique, the interfering beams travel through a nearly identical path. The

changes in the refractive index of the air mass would affect both beams equally and thus maintain the relative phase difference between the beams. This would be true as long as the spatial variation of the refractive indices in the air mass is smaller than S, the separation of the interfering point radiators.

There are also other advantages in utilizing the local reference beam technique. In order for two light beams to interfer, their path difference must be less than the coherent length of the illuminating light source. For a He-Ne laser, the coherence length is typically about 40 cm. In making a conventional hologram, a precise prior knowledge of the target range would therefore be necessary such that the light path can be equalized. Since the target is supposed to be obscured, this information cannot be assumed available. Moreover, even if the target range is known, the depth of the target field must be restricted to that of the coherent length. With the local reference beam technique, the path lengths of the two interfering beams would automatically equalize since they are generated from point radiators on the same surface. For the same reason, the target field can be of any depth. For most applications, a light source with a coherent length of less than 1 cm would provide adequate temporal coherence. This would allow a much greater choice of light sources, making it feasible to utilize devices such as laser diodes and CO_2 lasers.

4.4 PERFORMANCE ESTIMATION

To determine the effectiveness of such a system in imaging through fog, we examined a specific system as illustrated in Figure 19. The bandwidth of the image obtained with the system would be $2d/\lambda L$ = 250 lines/mm and the modulation frequency is equal to $\sin \theta/\lambda$ = 540 lines/mm. The optical processing arrangement shown earlier in Figure 14(a) is used to perform the spatial filtering. The zero order and the modulation terms are separated by the diffraction of

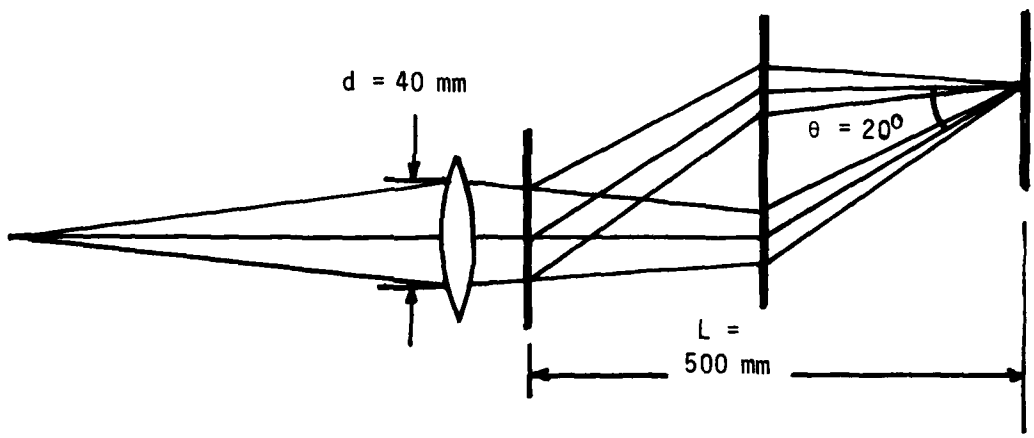

FIGURE 19. DIMENSIONS OF GRATING INTERFEROMETER

the converging beam. Bandpass filtering is accomplished by setting the lens aperture according to the image bandwidth. To assure maximum fringe contrast, the exposure should be made such that the recording is biased at a point where the material exhibits the highest transfer characteristic (i.e., the region with the steepest slope in the T_A-E curve). For example, with Kodak 649F plate as the recording material, the plate should be exposed to give an average transmittance of $T_A = 0.5$. The percentage of input light diffracted to one of the sidebands would be about

$$\left[\frac{T_A \beta H(\omega) A^2}{2(A^2 + B^2)}\right]^2 \times 100\% \qquad (4\text{-}11)$$

where β is the slope of the transfer characteristic at T_A and $H(\omega)$ is the frequency response. For 649 F plates, $\beta = 1.25$ at $T_A = 0.5$ and $H(\omega) = 0.8$ at $\omega = 500$ lines/mm. If the imaging process between the input transparency and the output plane is one-to-one, then the intensity of the speckled target image would be equal to

$$I_T = 0.0625 \left(\frac{A^2}{A^2 + B^2}\right)^2 \frac{P}{S} \text{ W/mm}^2 \qquad (4\text{-}12)$$

where P is the input light power and S is the total area of the input transparency illuminated. Although this is only a first order approximation, it provides a good estimate of the input image intensity when $B^2 >> A^2$ (i.e., very small input modulation).

The main source of noise at such a high diffraction angle is the scattering noise of the photographic plate. For 649F, at 540 lines/mm and $T_A = 0.5$, the power of the scattering noise is about 3×10^{-9} P W/line/mm^2. If the filter bandwidth is made to be equal to the signal bandwidth, that is 250 lines/mm, the total noise power that is transmitted to the output plane would be

$$3 \times 10^{-9} \times \pi\left(\frac{250}{2}\right)^2 P \text{ watts}$$

Since the noise power is evenly distributed across the image area S, the intensity of the scattering noise would be equal to

$$I_S = 1.47 \times 10^{-4} \frac{P}{S}$$

The SNR of the processed image would therefore be

$$I_T : I_S = 0.0625\left(\frac{A^2}{A^2 + B^2}\right)^2 : 1.47 \times 10^{-4} \qquad (4\text{-}13)$$

corresponding to an output contrast of

$$C_{out} = \frac{0.0625\left(\frac{A^2}{A^2 + B^2}\right)^2}{2(1.47 \times 10^{-4}) + 0.0625\left(\frac{A^2}{A^2 + B^2}\right)^2} \times 100\,\% \qquad (4\text{-}14)$$

For $B^2 >> A^2$, we may make the following approximation

$$\frac{A^2}{A^2 + B^2} \simeq \frac{A^2}{B^2} \text{ and } \frac{A^2}{A^2 + 2B^2} \simeq \frac{A^2}{2B^2}$$

The output contrast C_{out} can then be written in terms of input contrast (as observed directly through the scattering medium) as

$$C_{out} = \frac{2.5 \times 10^{-5}\, Cin^2}{2.94 \times 10^{-4} + 2.5 \times 10^{-5}\, Cin^2} \times 100\,\% \qquad (4\text{-}15)$$

where

$$C_{in} = \frac{A^2}{A^2 + 2B^2} \times 100\,\%$$

We plotted in Figure 20 the estimated contrast of the processed image as a function of the input contrast. We find that the processed

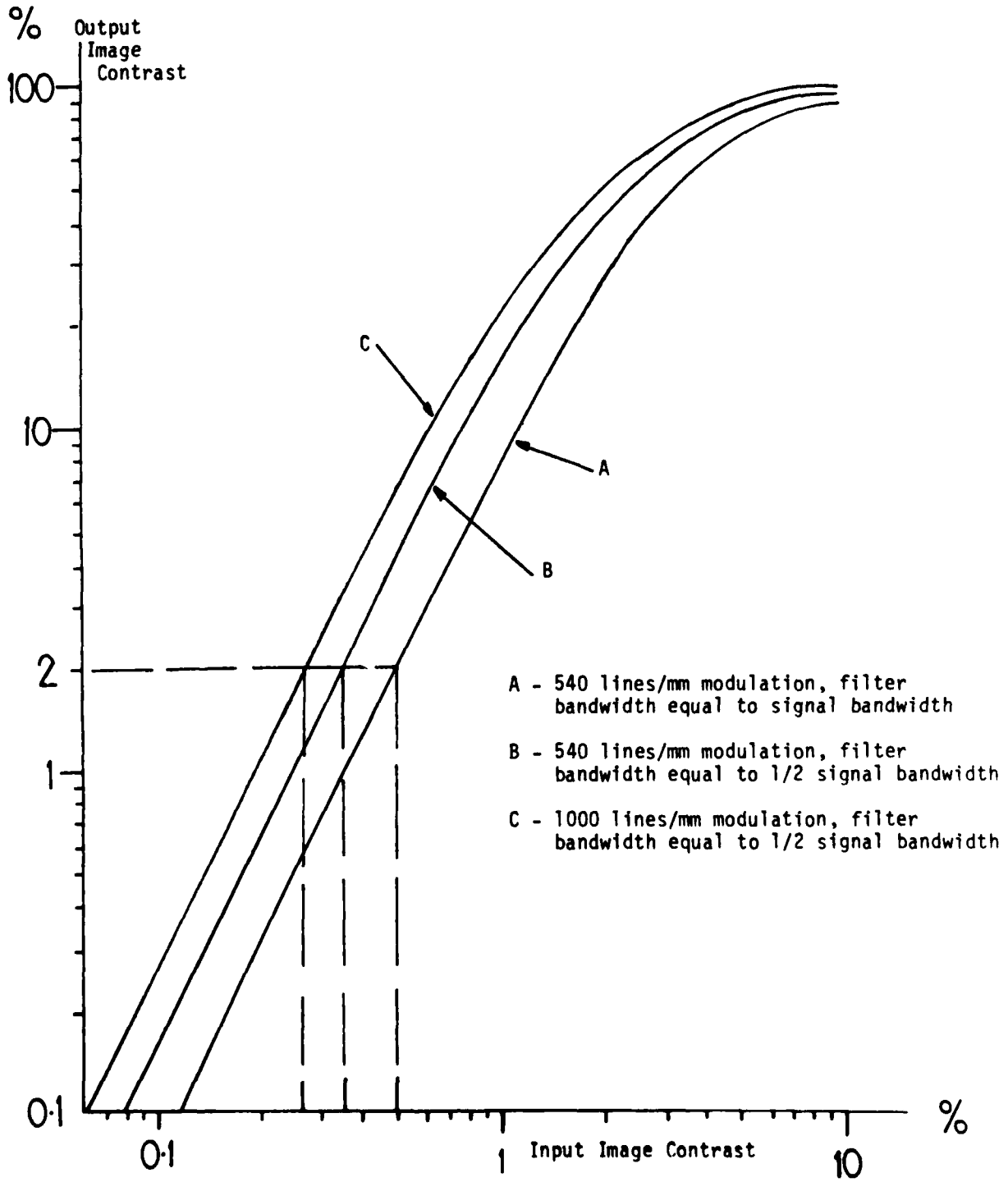

FIGURE 20. ESTIMATED SYSTEM PERFORMANCES

image would be recognizable by a human observer if the input image contrast is 0.5% or higher. Another indicator of system performance is the break even point. A positive gain in image contrast would be obtained if the input image contrast is greater than 0.12%.

To improve the performance of the system, the simplest way is to decrease the filter bandwidth. We note that the noise power is evenly distributed across the filter passband while the power of the image spectrum decreases linearly from the center frequency. Thus, if we decrease the filter bandwidth by half, the noise power would be cut by a factor of 4 while the signal power would only be lowered by a factor of 2. The resulting SNR would effectively be doubled. The performance of the system using a filter bandwidth half the size of the signal spectrum is also plotted in Figure 20. The processed image will be recognizable with an input image contrast as low as 0.35% and the break even point is reduced to 0.05%. Reducing the filter bandwidth would also produce a marginal loss in image resolution. Nevertheless, the available resolution would still be higher than needed in most applications, especially if the output is to be displayed on a TV screen. The marginal loss in resolution would generally be an acceptable trade-off for better SNR.

To further improve the SNR, we can increase the modulation frequency. For example, in Figure 20, we plotted the system using a 1000 lines/mm modulation frequency. A human observer would be able to recognize the processed image if the input image contrast is 0.28% or higher. However, we cannot continuously obtain a SNR improvement by increasing the modulation frequency. The finite frequency response of the recording material would place a limit on the modulation frequency as illustrated earlier in Figure 13. With Kodak 649F as the recording material, the optimum modulation frequency is around 1000 lines/mm, corresponding to a diffraction angle of 40° for 0.6328 μm illumination. Other factors also impose additional restraints on the modulation frequency of the grating. The grating become more

angularly selective with frequency. That is, the diffraction efficiency falls quickly as the incoming beam moves off the Bragg angle. This would produce a decrease in the intensity of image points away from the optical center, resulting in a reduction of the field of view. Furthermore, at high diffraction angles, the off-axis aberrations are more severe. The problem of aberrations will be discussed in a later section.

The use of the local reference beam technique makes the holographic system practical in field conditions. However, a price in SNR is paid in gaining these advantages. Comparing Eq. 3-3 and Eq. 4-3, we see that with the conventional holographic technique, $|f(x, y) * h(x, y)|$ is reconstructed. While, with the local reference beam technique, $|f(x, y) * h(x, y)|^2$ is reconstructed. Since the bandwidth of $|f(x, y) * h(x, y)|^2$ is twice as wide as $|f(x, y) * h(x, y)|$, the SNR would be a factor of 4 lower for the local reference beam technique. If the filter bandwidth is set to be half of the signal bandwidth, then the SNR loss would be reduced to a factor of 2. Thus, the conventional holographic technique should be used whenever the experimental conditions allow

4.5 RECORDING MATERIAL

The quantitative analysis presented in the previous section applies only to the chosen recording material, the Kodak 649F spectroscopic plate. The 649F plate was chosen because of its common usage in holography. Its performance would serve well as a standard with which other materials may be compared.

Upon choosing a recording material for the interferometric imaging system, the optimum modulation frequency and optimum exposure must then be determined. The optimum modulation frequency is obtained by measuring the SNR as a function of spatial frequency. For 649F, the optimum modulation frequency is around 1000 lines/mm as shown in Figure 21. The optimum exposure can be similarly determined

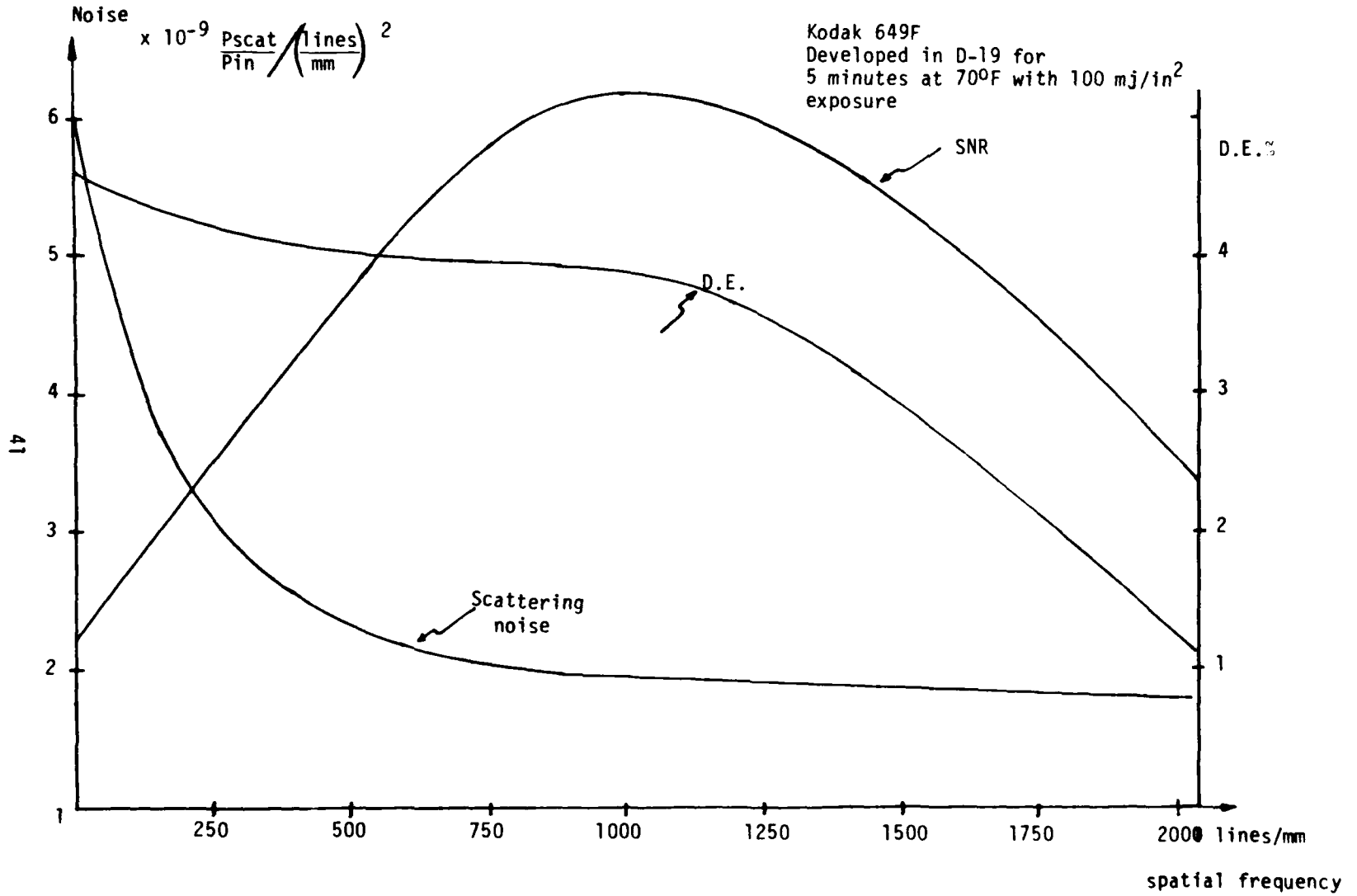

FIGURE 21. CHARACTERISTICS OF 649F PLATES AS A FUNCTION OF SPATIAL FREQUENCY

by measuring the SNR as a function of exposure. The behavior of 649F as a function of exposure under 0.6328 μm illumination is plotted in Figure 22. The optimum exposure is achieved at about 100 $\mu J/cm^2$. It should be noted that the SNR measurements are dependent on the modulation depth of the input signal. For an input with high modulation, the film nonlinearity will produce intermodulation noise that cause the optimum exposure to occur at a lower exposure level. In order to obtain optimum parameters appropriate for our present application, the SNR measurements were made using a fringe pattern with fairly low modulation (28%).

One of the most serious drawbacks of using 649F is its low sensitivity. In situations where the input light intensity is very low, the required exposure time would be impractically long. Various techniques may be used to increase the speed of the emulsion. For example, by soaking the photographic plate in water for about 15 minutes inside a liquid gate before the exposure, the sensitivity of the emulsion can be increased by as much as 4 times. The use of special development procedure may increase the speed by another factor of 2. However, to improve the system sensitivity significantly, the substitution with a faster recording material would be necessary.

Another fine grain holographic recording material is the Kodak 131 plate. The optimum exposure for the 131 plate is about 500 nJ/cm^2, making it 200 times faster than the 649F plate. Another possible substitution is the Kodak AHU5460 microfilm. The film has a low noise acetate substrate and it has been utilized for many years in the recording of data for optical processing of synthetic aperture radar (SAR) signals. The optimum exposure for the 5460 microfilm is about 100 nJ/cm^2. However, to make a photographic emulsion more sensitivity, it is necessary to use larger silver halide crystals. The larger grain size would produce more severe grain noise. Thus, a tradeoff between sensitivity and SNR exists and the choice of the recording material would depend on the requirements of the specific application.

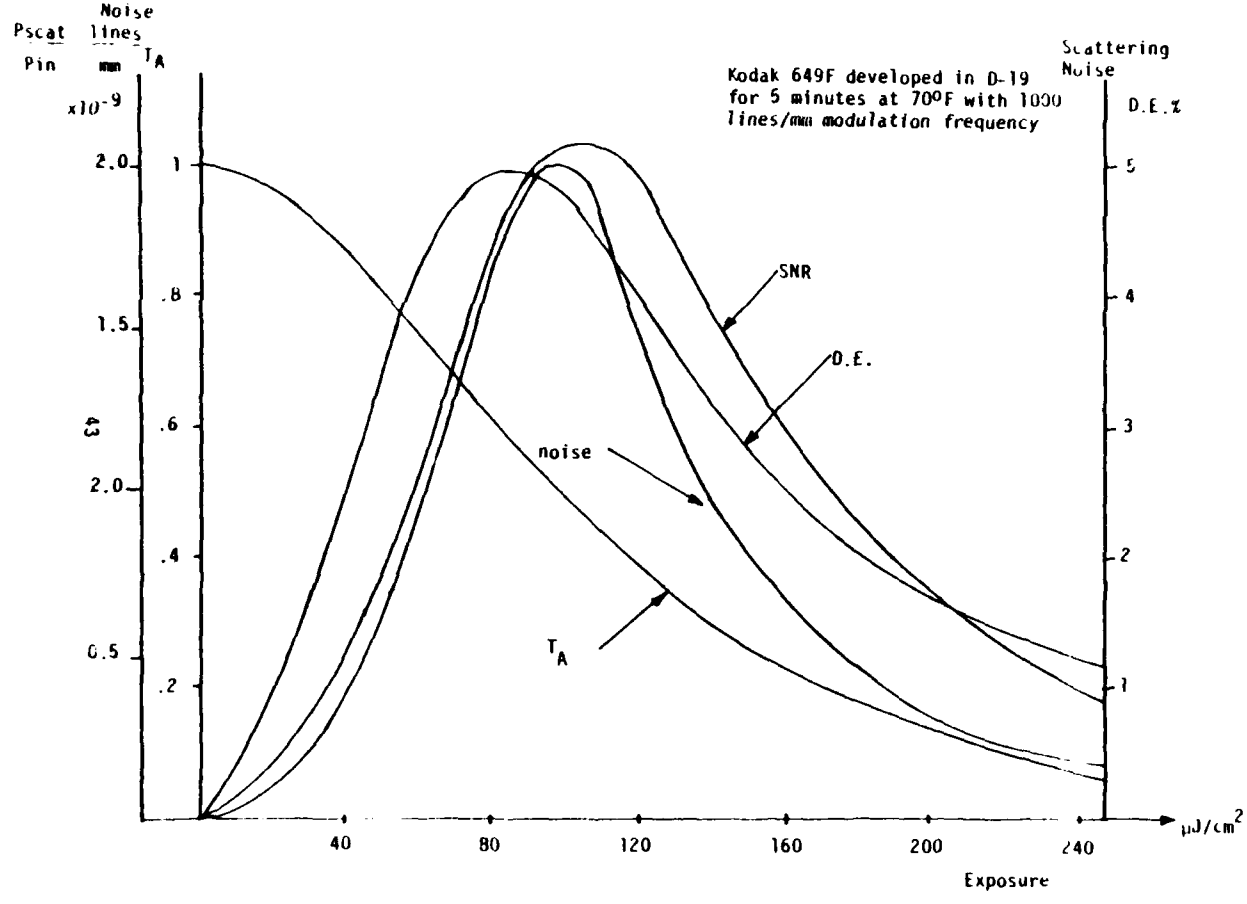

FIGURE 22. CHARACTERISTICS OF 649F PLATES AS A FUNCTION OF EXPOSURE

Like all silver halide photographic material, 649F requires chemical developments. The normal development process requires about 8 minutes (5 minutes development and 3 minutes fixation). The development time can be shortened by the use of a higher development temperature, a faster acting developer or a higher concentration of hydroxide in the developer. It is possible to reduce the processing time to less than a minute. However, rapid development usually results in a lower quality recording. The developed silver grains tend to clump together and concentrate near the emulsion surface. The result is a higher scattering noise and poorer uniformity.

To substantially reduce the processing time, it would be necessary to use a real time light modulator in place of the photographic material. Unfortunately, most real time light modulators such as PROM[9] and liquid crystal light valves[10] are sensitive predominantly in the blue-UV region. The photoplastic device has been shown to be sensitive to near IR illumination, responding up to 1.15 μm and its sensitivity is compatible with that of the 649F plate[14]. However, the achievable SNR is lower[15].

When a photographic material is used with the system, the optical processing should be performed with the plate or film inside a liquid gate. The emulsion surface is not flat and the random thickness variation across the emulsion would introduce additional scattering noise. By placing the film inside a liquid whose refractive index matches that of the emulsion, the effect of the irregular surface relief can be eliminated. Xylene with a refractive index of 1.5 is the most commonly used liquid. It matches particularly well acetate based film such as the 5460 microfilm.

For the best combination of sensitivity, processing speed and SNR the photographic plate or film can be placed inside a liquid gate filled with water. The film is exposed while it is inside the water gate and the film is then taken out for development. (It is also possible to develop the film in situ by replacing the water with

developer.) After a brief fixing period (just enough to clear the film), the developed transparency is placed right back into the water gate for optical processing. Placing the film inside the water gate before the exposure increases the film sensitivity. Presoaking the emulsion would also facilitate the penetration of the developer, resulting in a faster and more complete development. Putting the developed film right back into the water gate eliminates the drying step. Although water, with a refractive index of 1.3, does not match the emulsion as well as xylene, a substantial amount of the surface relief effect can still be eliminated.

4.6 IMAGE ABERRATIONS AND DESIGN PARAMETERS

In this section, we shall examine the design parameters for a grating interferometer that will produce minimum image aberrations. First, let us consider the case where a sinusoidal plane grating is placed normal to the optical axis of the imaging system and examine how well it can image an object point located at the optical center. One approach is to use the ray tracing technique to determine the shape and location of the image formed by the diffracted light.

A light ray with directional cosines cos θx and cos θy impinging on the grating will emerge as 3 rays, the ± first order and the zero order. Only one of the first order diffracted rays is of interest to us. The directional cosines of this diffracted ray can be determined by

$$\cos \theta_x = \cos \phi_x - \frac{\lambda}{dy}$$

and

$$\cos \theta_y = \cos \theta_y - \frac{\lambda}{d_y}$$

where dx and dy are the fringe spacings in the corresponding direction.

In Figure 23(a), we show the ray trace for the point image formed by the diffracted light. We see that the point image is severely aberrated. In Figure 23(b), we show the experimentally obtained light distributions at three different image planes. Coma and astigmatic aberration is quite evident. An alternate approach in examining the image aberration is to consider the grating as a hologram constructed with two point sources located at infinity (i.e., plane waves). The hologram is then reconstructed by a converging beam that focuses at a distance R_c from the plate. If we confine the reference beam, the object beam, the reconstructing beam and the image beam all in the x-z plane, the reconstructed point image is found to be located at a distance R_i from the center of the plate as illustrated in Figure 24, where R_i is determined by

$$\frac{1}{R_i} = \frac{1}{R_c} - \left(\frac{1}{R_o} - \frac{1}{R_r}\right)$$

Since $R_o = R_r = \infty$, we have $R_i = R_c$.

The wavefront derivation (in wavelengths) is computed by Champagne[11] to be

$$\Delta = \frac{1}{\lambda}\left[-\frac{1}{8}(x^4 + y^4)S + \frac{1}{2}(x^2 + y^2)xC_x - \frac{1}{2}(x^2 A_x)\right]$$

where

$$S = \frac{1}{R_c^3} - \left(\frac{1}{R_o^3} - \frac{1}{R_r^3}\right) - \frac{1}{R_i^3} \qquad (4\text{-}19)$$

(spherical aberration)

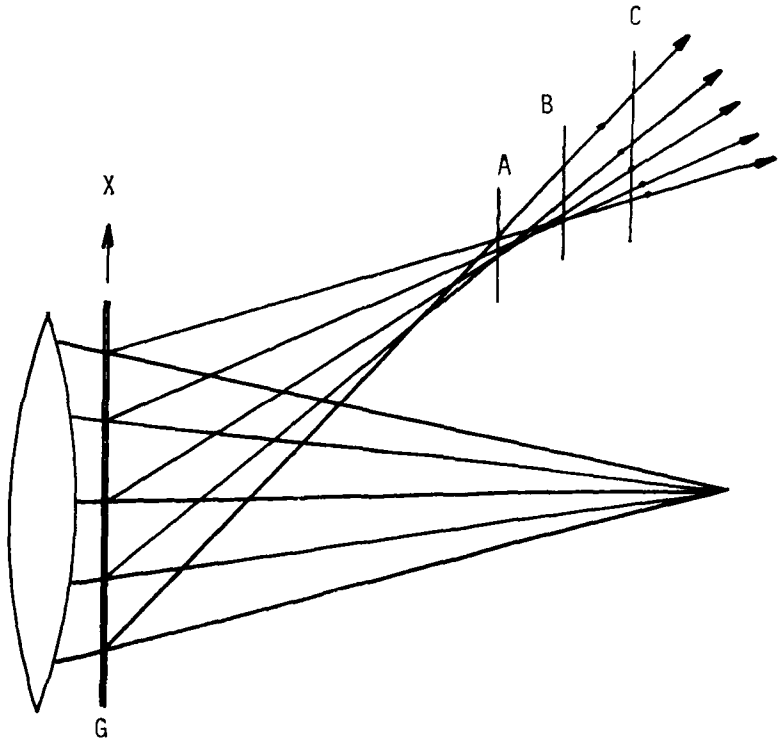

A B C

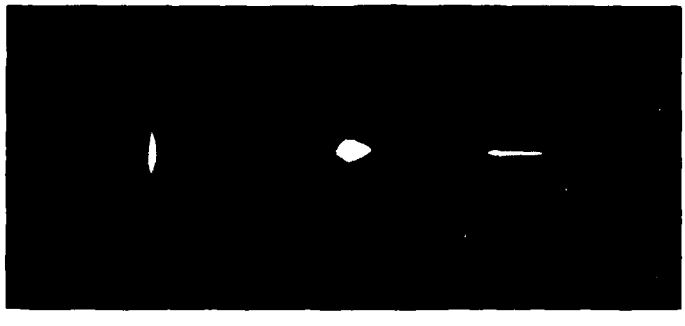

FIGURE 23. ABERRATIONS OBTAINED WITH A PLANE GRATING PLACED NORMAL TO OPTICAL AXIS

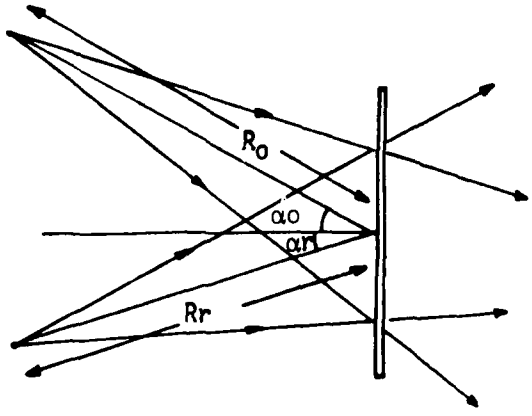

FIGURE 24A. GRATING CONSTRUCTION GEOMETRY

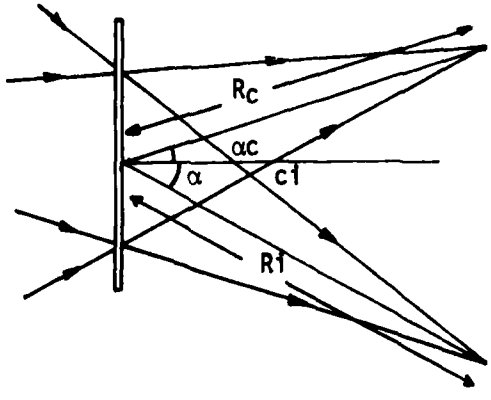

FIGURE 24B. GRATING DIFFRACTION GEOMETRY

$$C_x = \frac{\sin \alpha_c}{R_c^2} - \left(\frac{\sin \alpha_o}{R_o^2} - \frac{\sin \alpha_r}{R_r^2}\right) - \frac{\sin \alpha_i}{R_i^2} \quad (4\text{-}20)$$

(coma)

$$A_x = \frac{\sin^2 \alpha_c}{R_c} - \left(\frac{\sin^2 \alpha_o}{R_o} - \frac{\sin^2 \alpha_r}{R_r}\right) - \frac{\sin^2 \alpha_i}{R_i} \quad (4\text{-}21)$$

(astigmatic aberration)

with $R_o = R_r = \infty$, they can be simplified to

$$S = \frac{1}{R_c^3} - \frac{1}{R_i^3} \quad (4\text{-}22)$$

$$C_x = \frac{\sin \alpha_c}{R_c} - \frac{\sin \alpha_i}{R_i} \quad (4\text{-}23)$$

and

$$A_x = \frac{\sin^2 \alpha_c}{R_c} - \frac{\sin^2 \alpha_i}{R_i} \quad (4\text{-}24)$$

Since $R_i = R_c$, we have $S = 0$; there would not be any spherical aberration. By placing the grating perpendicular to the optical axis of the reconstructing beam, $\alpha_c \approx 0$, and we have

$$C_x = \frac{\sin \alpha_i}{R_i} \text{ and } A_x = \frac{\sin^2 \alpha_i}{R_i} \quad (4\text{-}25)$$

The image would therefore suffer from coma and astigmatic aberration. We can see that the aberration increases with the diffraction angle and astigmatism is the more dominant aberration.

From Eqs. 4-23 and 4-24, we also find that the aberrations can be made to vanish by making $\alpha_c = \alpha_i$. This can be achieved by tilting the grating an angle $\alpha_i/2$. In Figure 25(a), we show the

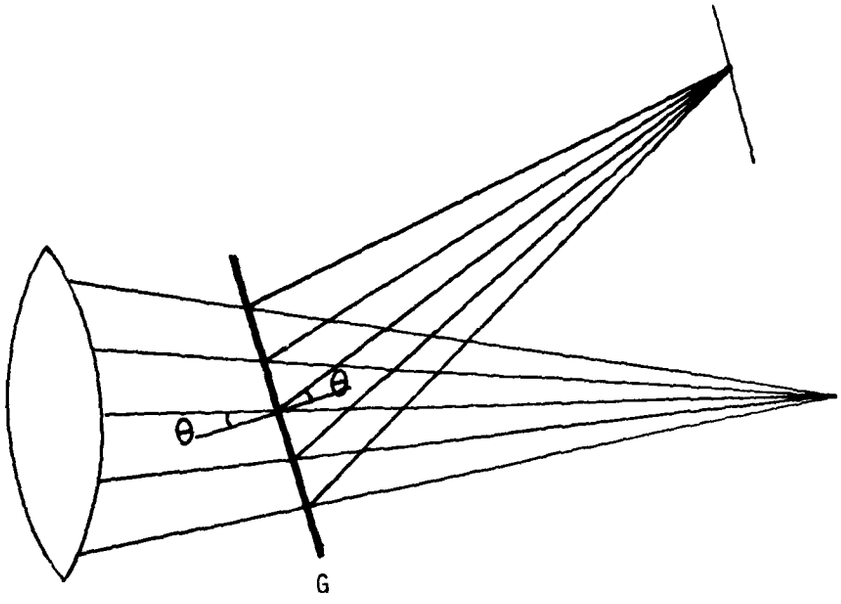

FIGURE 25A. CORRECTION OF ABERRATION BY TILTING GRATING

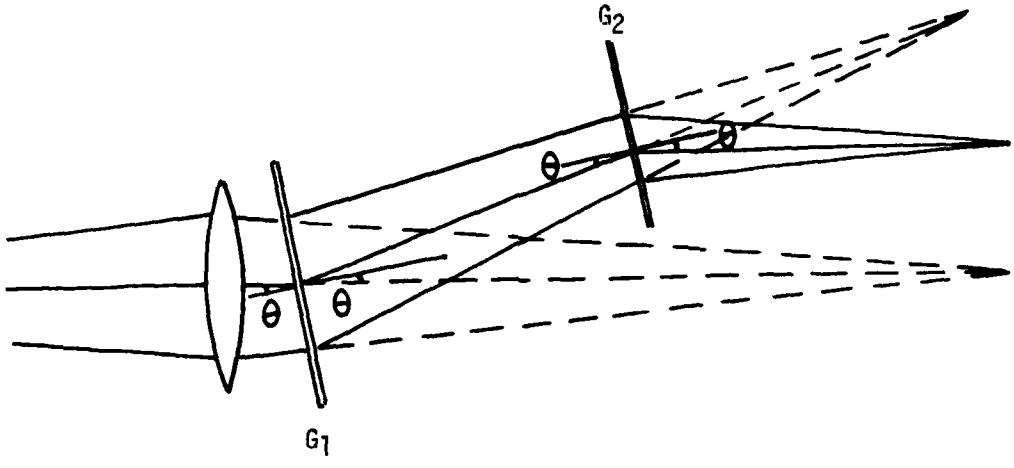

FIGURE 25B. ABERRATION CORRECTION FOR A CONVERGING BEAM DIFFRACTED BY TWO GRATINGS

ray trace with the tilted grating arrangement. The aberrations indeed disappear.

What we have described would apply directly to the lower branch of the grating interferometer. The upper branch on the other hand, is diffracted twice. By tilting both gratings by an angle $\alpha_1/2$, the aberrations will be corrected as illustrated in Figure 25(b). Since the required angle of tilt for the second grating is the same with the upper and lower branches of the interferometer. A single solid grating can therefore be used. In order for the images reconstructed by both branches to coincide, the central rays should form a parallelogram. Together with the angle requirements, an aberration-free grating interferometer can be designed with two sinusoidal gratings as shown in Figure 26.

The use of plane gratings is not very efficient since one-third of the light is diffracted to the conjugate order. The use of volume gratings would confine the diffraction to a single order. By making the first grating to have a diffraction efficiency of 50%, and the second to have a diffraction efficiency of 100%, all the transmitted light energy would be directed to the image plane. The tilted grating arrangement can also be used with volume gratings to produce aberration-free images. However, if the grating is constructed with two plane waves, the bragg condition would be satisfied fully by only the central rays as illustrated in Figure 27(a). The peripheral rays would be diffracted less efficiently. The result is a reduction in the effective aperture of the imaging system in the direction of diffraction. This effect is particularly pronounced when a high diffraction angle is used with a fast lens. To avoid this effect, a volume grating that is constructed with two point sources instead two plane waves should be used. The volume grating is placed with its back to the impinging converging light beam as illustrated in Figure 27(b). The bragg condition will be satisfied across the entire aperture.

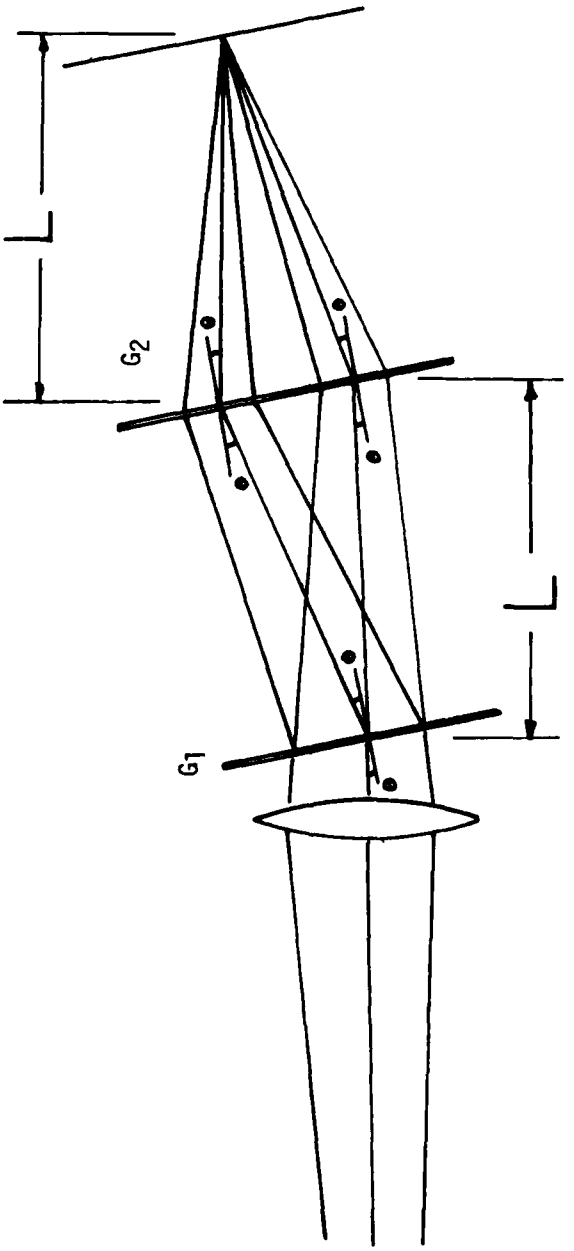

FIGURE 26. AN ABERRATION FREE IMAGING GRATING INTERFEROMETER

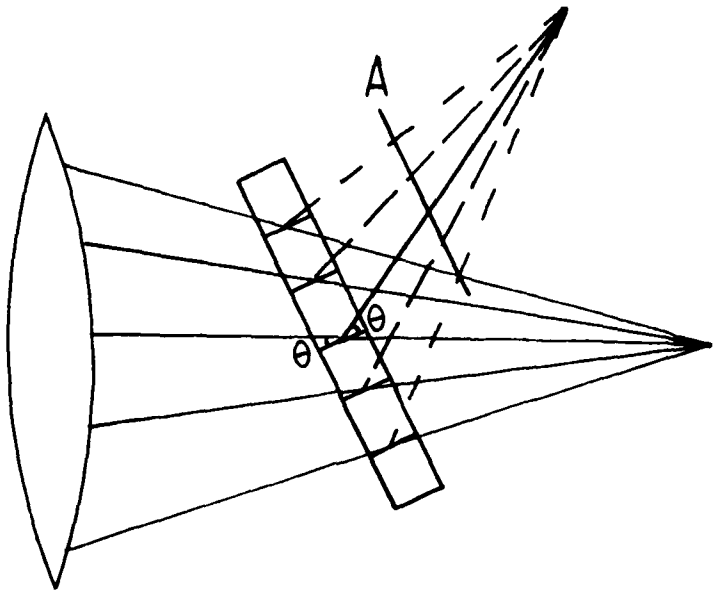

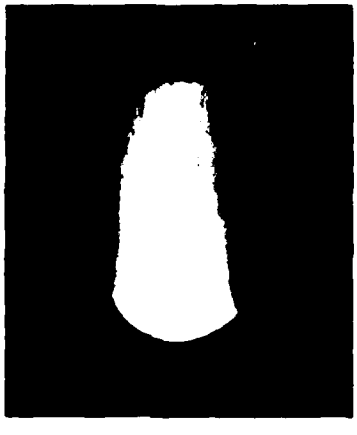

FIGURE 27A. DIFFRACTION OF A CONVERGING BEAM WITH A GRATING CONSTRUCTED WITH PLANE WAVES.

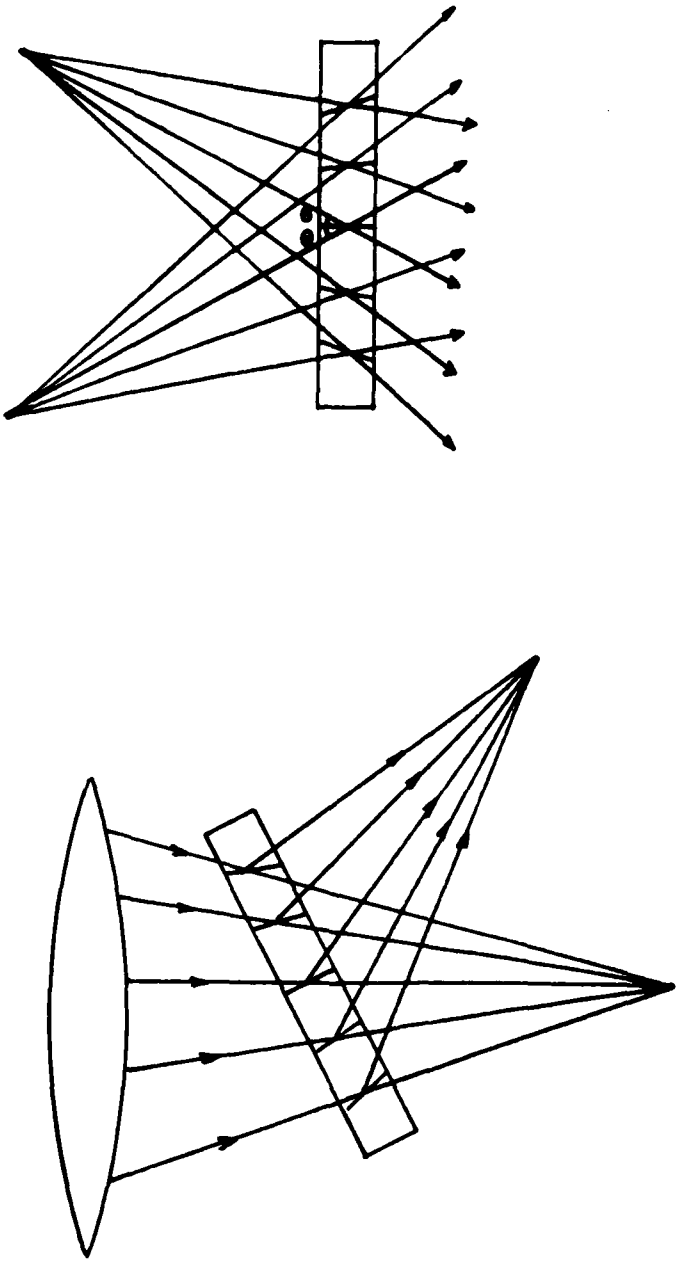

FIGURE 27B. DIFFRACTION OF A CONVERGING BEAM WITH A GRATING CONSTRUCTED WITH TWO DIVERGING BEAMS.

With these preliminary discussions, we can now proceed to describe the optical arrangement that was used to fabricate the gratings utilized in our interferometer.

4.7 GRATING FABRICATIONS

The arrangement for fabricating the first grating is rather simple. Two point sources, placed symmetrically with respect to the holographic plate are located at a distance L from the center of the plate. L is determined by the desired grating position in the interferometer as shown in Figure 28 (a). When the developed holographic grating is placed at the appropriate position behind the imaging lens, the converging beam will be diffracted to form an unaberrated point image as shown in Figure 28 (b).

To generate the second grating, we make use of the same two point sources as the first grating, and add a third point source mid-way between them. The location of this third point source will determine the eventual image position in the grating interferometer. The holographic plate is placed midway between the first grating and the image plane such that the central rays of the interferometer will form a parallelogram. The light emanated from this third point source must have a wide enough divergence to cover the entire holographic plate. This would require a lens with an impossibly large numerical aperture. To overcome this problem, we use a lens with a numerical aperture slightly larger than that of the imaging lens and focus a beam onto a volume grating. This volume grating should have a spatial frequency identical to that of the first grating and a diffraction efficiency of 50 % (or we may simply make use of the first grating that was generated). The undiffracted beam will diverge and illuminate the region of the plate where the upper point source is also illuminating. The diffracted light on the other hand, will be directed towards the lower portion of the plate that is illuminated by the lower point source as illustrated in Figure 30(a). Recorded

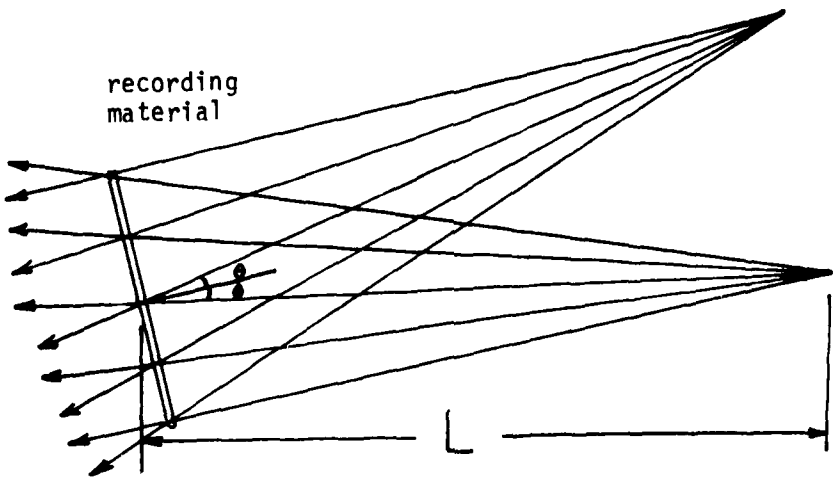

FIGURE 28A. FABRICATION OF FIRST GRATING

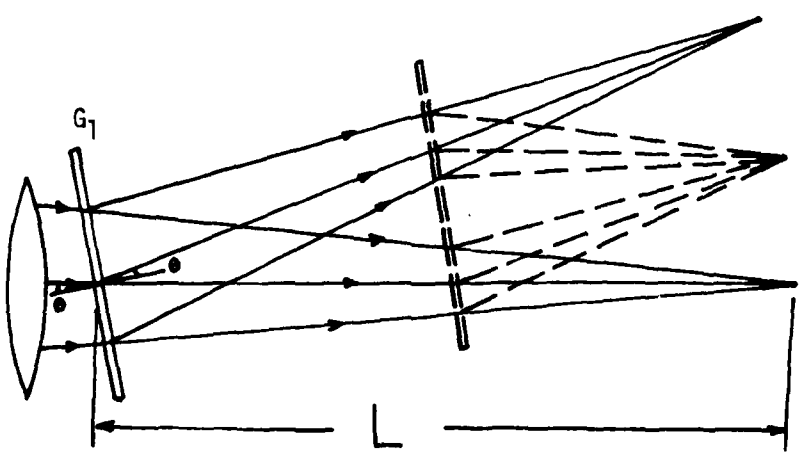

FIGURE 28B. DIFFRACTION OF A CONVERGING BEAM BY FIRST GRATING

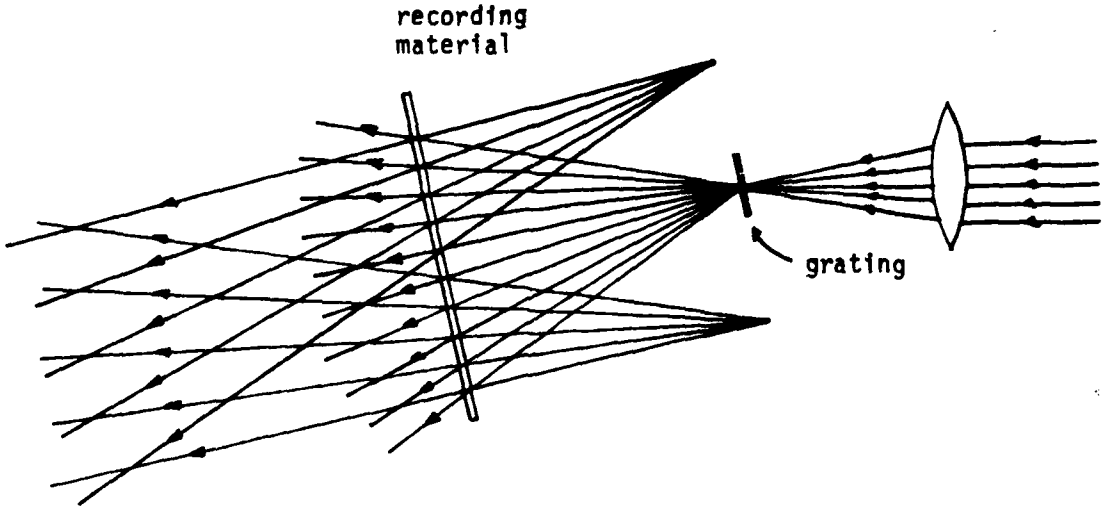

FIGURE 29A. FABRICATION OF SECOND GRATING

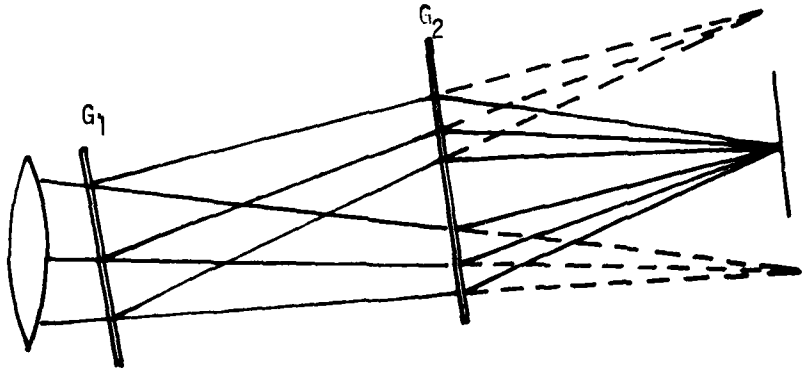

FIGURE 29B. IMAGING GRATING INTERFEROMETER

on the holographic plate will be two separate sets of fringe patterns. The spatial frequencies of these two patterns are the same but the fringes are tilted differently. After the plate is developed, we can assemble with the two gratings an interferometer as shown in Figure 29(b). The interferometric system will be able to produce the image of an on-axis point object without any aberration.

To generate the gratings, dichromated gelatin was used as the recording material. Dichromated gelatin is the best holographic recording material available today[12-13]. The maximum achievable diffraction efficiency is over 90% with most of the optical loss due to absorption. Since the gelatin is grainless, the material also has the advantage of low noise. The scattering that exists with dichromated gelatin is due to microscopic cracks in the gelatin caused by the dehydration operation. Nevertheless, the noise behavior is superior even to an unbleached 649F plate.

The gelatin layer can be coated on a glass substrate by dip-coating. However, photographic materials with a thick emulsion offer a convenient source of high quality gelatin coatings. The familiar Kodak 649F plate was used to generate our gratings. The gelatin layer is prepared by first dissolving all the silver halide crystals in the gelatin with a fixer. The plate is then conditioned and dichromated. After the exposure, the dichromated gelatin plate is developed by dehydration with alcohol baths. The preparation and development procedures for dichromated gelatin plates are listed in Tables 4-1 and 4-2.

The diffraction efficiency of the gratings can be controlled by varying the exposure or K-ratio in the recording. The first grating in our interferometer both diffracts and transmits 40% of the input light. The rest is lost due to absorption, scattering, and reflection. The second grating has diffraction efficiency of 75%. Thus, the overall efficiency of the grating interferometer is about 60%.

TABLE 4-1
PREPARATION OF DICHROMATED GELATIN PLATES
BASED ON 649F

	DIRECTION	
1.	Soak in fixer without hardener for 10 minutes	Room light
2.	Wash in running water at 90°F for 5 minutes; start at 68°F and raise temperature gradually to 90°F; following wash, lower temperature at same rate to 68°F.	Room light
3.	Soak in fixer with 3.25% hardener for 10 minutes	Room light
4.	Wash in running water for 10 minutes	Room light
5.	Rinse in distilled water for 5 minutes	Room light
6.	Dip into a Photo-Flo 200 solution (2 drop/liter) for 30 seconds and remove excess with sponge	Room light
7.	With plate in horizontal position, dry overnight at room temperature	Room light
8.	Soak in 5% ammonium-dichromate solution with 2 drops/liter of photo-flow 200 for 5 minutes	Red light
9.	With plate in horizontal position, dry overnight at room temperature	Red light

TABLE 4-2
STANDARD DEVELOPMENT OF DICHROMATED GELATIN PLATES

	DIRECTION	
1.	Soak in 0.5% solution of ammonium dichromate for 5 minutes	Red light
2.	Soak in fixer with 3.25% hardener for 5 minutes	Red light
3.	Wash in running water for 10 minutes	Room light
4.	Soak in distilled water for 2 minutes with agitation	Room light
5.	Dehydrate in a 50/50 solution of distilled water and isopropanol for 3 minutes	Room light
6.	Dehydrate in 100% isopropanol for 3 minutes	Room light
7.	Free-air dry for at least 1 hour	Room light
8.	Remove water completely from emulsion by baking or with a vacuum chamber	Room light

4.8 WIDEFIELD GRATING INTERFEROMETER

A system fabricated with the technique we just described would be capable of imaging any object point on the y-axis perfectly. However, for the object points that are located away from the y-axis, the image would be aberrated.

We have shown that all the aberrations can be eliminated if we make $\alpha_i = \alpha_c$ and we designed a system that will provide aberration free performance for an object point at the optical center. The image will remain unaberrated as the object point moves away from the optical center along the y-axis. The condition that $\alpha_i = \alpha_c$ will continue to be satisfied. If the object point moves off the y-axis however, the point image will suffer from coma and astigmatic aberration as illustrated in Figure 30. The amount of aberrations would be proportional to

$$\frac{\sin(\alpha_c + \Delta\alpha)}{R_c^2} - \frac{\sin(\alpha_i - \Delta\alpha)}{R_i^2} \qquad (4\text{-}26)$$

For coma

and

$$\frac{\sin^2(\alpha_c + \Delta\alpha)}{R_c} - \frac{\sin^2(\alpha_i - \Delta\alpha)}{R_i} \qquad (4\text{-}27)$$

For astigmatic aberration

where $\Delta\alpha$ is the corresponding entrance angle of the off-set object point in the x-direction. We can see that the aberrations increase with $\Delta\alpha$. Thus, the image points at the edge of the image field would be more severely aberrated than those near the center of the field. Furthermore, we find that coma decreases with α_c while astigmatism increases with α_c for a given $\Delta\alpha$. The effect of astigmatic aberration nevertheless dominates and a grating with a higher spatial frequency would be more sensitive to $\Delta\alpha$.

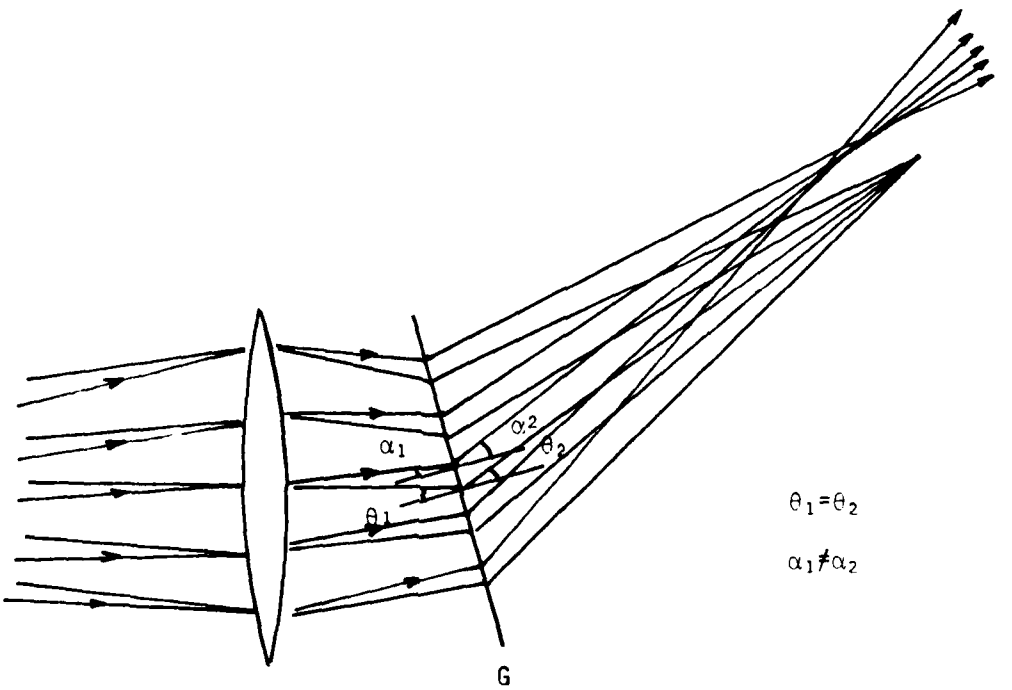

FIGURE 30. ABERRATION OF AN OFF AXIS DIFFRACTION

In most Army applications, the grating interferometer would be utilized with a telephoto imaging system. The field of view (or field angle) would generally be limited and the off-axis aberration would not be significant enough to be a problem. However, if the application demands a large field angle, a wide field grating interferometer can be constructed with the use of computer holographic techniques. In the following, we shall briefly describe the concept and fabrication procedure for a wide field grating interferometer.

For each field angle, we can compute the necessary phase transformation $\phi_n(\rho, \theta)$ to produce an unaberrated image. For example, for an object point δ_n, we can propagate the light wave to the plane where the hologram is to be located and compute phase distribution of the wavefront $\phi_{n,in}(\rho, \theta)$ at that plane. Similarly, we can propagate the light wave (backward) from the corresponding image point to the hologram plane and obtain the necessary wavefront $\phi_{n,out}(\rho, \theta)$ to produce an unaberrated image point. The required phase transformation for producing a point image at δ_n would be

$$\phi_n(\rho, \theta) = \phi_{n,out}(\rho, \theta) - \phi_{n,in}(\rho, \theta) \qquad (4\text{-}28)$$

After computing the phase transformation $\phi_n(\rho, \theta)$ for a representative set of object points in the field of view, we can then obtain an average phase transformation function

$$\phi(\rho, \theta) = \frac{1}{N} \sum_{n=1}^{N} \phi_n(\rho, \theta) \qquad (4\text{-}29)$$

It has been shown that a hologram that provides such a phase transform will produce the smallest mean squared phase error over the entire field of view [20]. The image point reconstructed would be slightly larger than a diffraction limited spot but the small spot size can be maintained over a much larger range of field angles[17].

To produce the necessary wavefront to construct a hologram that gives the desired phase transformation $\phi(\delta, \theta)$, a computer generated hologram can be used[16]. A computer generated hologram (CGH) represents the amplitude and phase of a wavefront at a particular sampled position by the size and position of a binary cell within a grid. However, the reconstruction efficiency of a CGH is quite low. And due to the limited space-bandwidth available with a computer display, the carrier frequency and numerical aperture of the CGH have to be severely restricted. Thus, instead of using the CGH itself in the grating interferometer, it is copied onto a dichromated gelatin plate as illustrated in Figure 32. We note that with such a scheme, the CGH is not constructed to produce the necessary wavefront $\phi(\rho, \theta)$ directly at the hologram plane, but it is made to produce a wavefront which upon propagating through the optical system, would become $\phi(\rho, \theta)$ at the recording plane[17].

4.9 EXPERIMENTAL RESULTS

Before the system was evaluated for imaging through a scattering medium, it was tested for its imaging ability using a resolution target as the object. The target transparency was diffusely illuminated from the back with a ground glass diffuser. In Figure 33(a), we show the input used in the evaluation and in Figure 33(b), we have the image obtained with the grating interferometric system. The image quality is very good with only a slight degradation at the edge of the field.

The image in Figure 33(b) was obtained at the plane where the two interfering images exactly coincide (i.e., $z = 0$ plane). In order to prevent the scattered light from forming stationary fringes the two images have to be slightly displaced or sheared. To obtain the correct amount of shearing, a back illuminated rotating diffuser

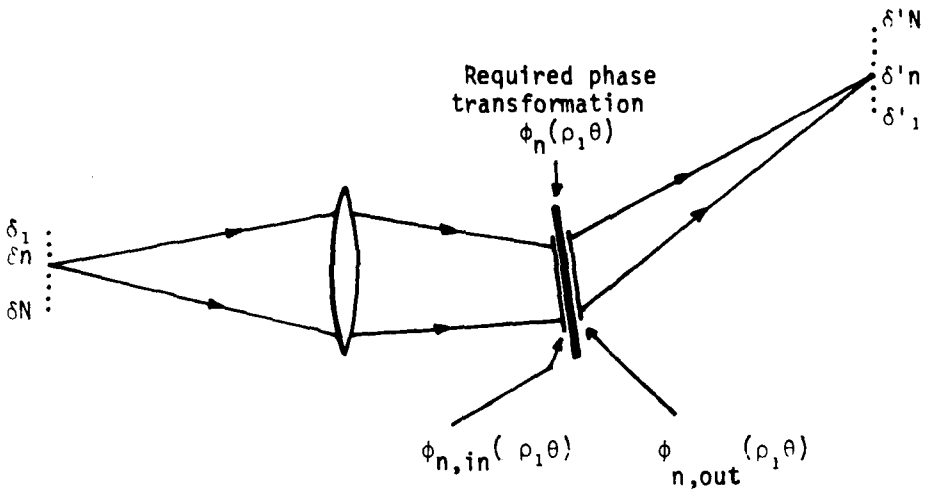

FIGURE 31. COMPUTATION OF REQUIRED PHASE TRANSFORMATION

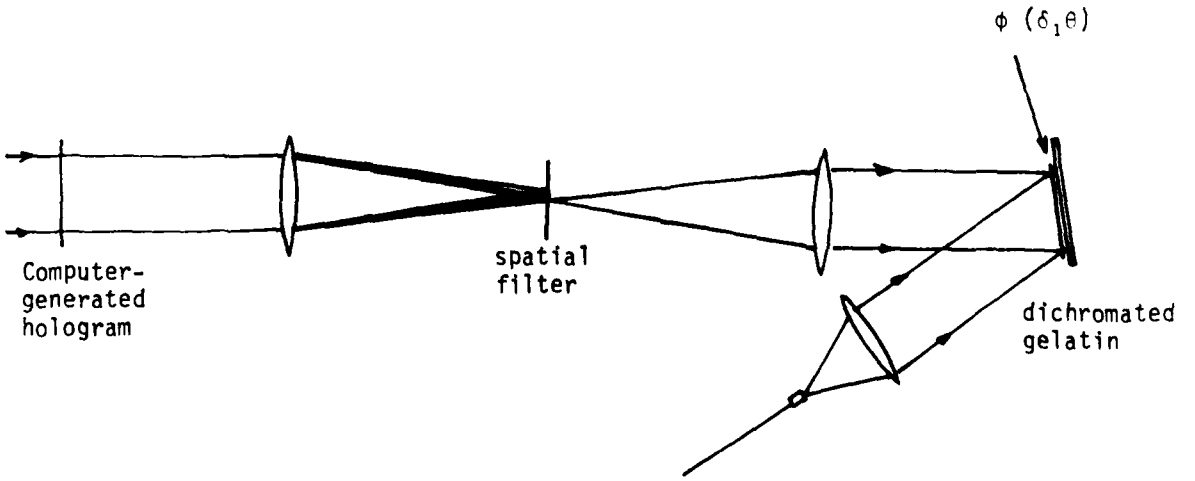

FIGURE 32. FABRICATION OF WIDE-FIELD DIFFRACTION GRATING

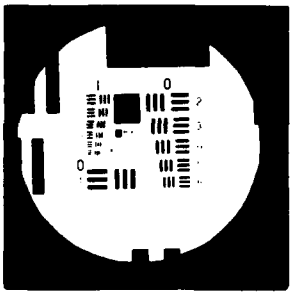

A
input

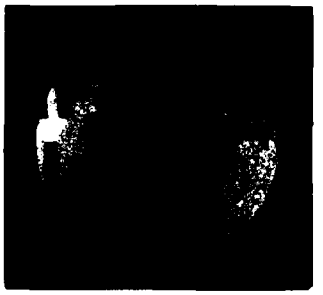

B
image

FIGURE 33. EVALUATION OF THE SYSTEM'S IMAGING ABILITY

was inserted between the target plane and the imaging lens. When the gratings are perfectly aligned, stationary fringes can be observed across the entire image field with a microscope. While observing the output light field, the second grating was displaced slightly in the z-direction until the fringes disappeared. Any further displacement of the grating would result in an excessive image blur.

To evaluate the system capability in imaging through scattering media, a qualitative test was first performed. A diffusely illuminated photographic transparency of a toy tank on a grass lawn was used as the target. To produce an adjustable scattering medium, a liquid crystal scattering plate was used. The scattering plate was constructed with a liquid crystal layer sandwiched between two glass plates. The liquid crystal was made to operate in the dynamic scattering mode with the application of an AC voltage. The amount of scattering can be made to vary by adjusting the excitation voltage. In order to create a rapid change in the scattering field, the scattering plate was mounted on a translator stage and translated across the light path during the exposure.

The excitation voltage was initially set at zero such that the liquid crystal plate was completely clear and image distinctly visible. The excitation voltage was then steadily increased until the target image contrast was so low that it was no longer recognizable. The target image was then recorded with the grating interferometric system and processed as described earlier. In Figure 34(a), we show the target image as observed directly through the scattering medium and in Figure 34(b) we show the processed image obtained with the interferometric system. We can see that the image contrast is significantly improved and the processed target image is easily recognizable.

To test the system under a more realistic simulated scattering environment, a glass water tank filled with diluted milk was used as

A
direct image

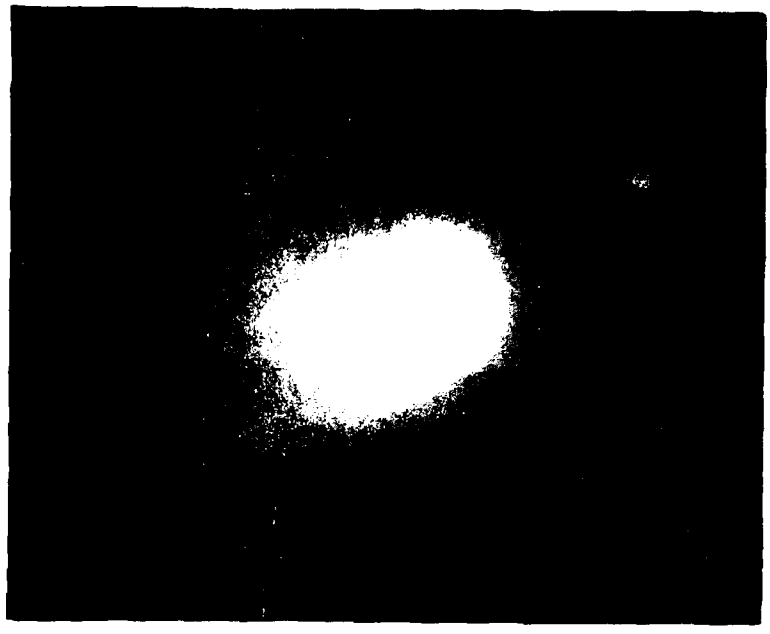

B
processed image

FIGURE 34. QUALITATIVE TEST WITH COMPLEX TARGET USING LIQUID CRYSTAL SCATTERING MEDIA AS SCATTERING MEDIUM

the scattering medium. The suspension of the fat particles in a 3-dimensional volume creates an environment very similar to that of natural fog. For this experiment, a toy tank, placed just outside the glass water tank and illuminated from the side, was used as the target. The concentration of the milk was gradually increased until the target was no longer recognizable. The target image was then recorded with the grating interferometric system. The processed image is shown in Figure 35. The target is easily recognizable as an army tank.

It is difficult to define the image contrast of a complex continuous tone target. Thus, to facilitate a quantitative evaluation of the system, we used a simple two-tone object as illustrated in Figure 36. When the input image contrast is very low, I_{max} and I_{min} would be very close in magnitude and it would be difficult to measure the input contrast accurately. To circumvent this problem, we simulated the effect of imaging through a scattering medium with the arrangement depicted in Figure 36. With such an arrangement, I_{min} (scattered light intensity) and $I_{max}-I_{min}$ (unscattered light intensity) can be measured separately by blocking the other beam. The relative intensities of signal and background light fields can be set to any ratio desired by adjusting the variable beam splitters.

To evaluate the system performance, the contrast of the input image was adjusted to 5%, 1%, 0.6%, and 0.4%. The image with 5% contrast was barely recognizable and the images with the lower contrasts were not visible at all. The processed image obtained with the interferometric system were 85%, 19%, 8.5%, and 3% respectively. The experimental results are plotted in Figure 37 together with the estimated performance computed earlier. To illustrate the clarity of the processed image, we show in Figure 38 (a) and (b), the direct input image and the processed output image. The contrast of the input image was only 1%, just below that required for human recognition. The processed image has a much improved contrast of 19%. It is clearly visible by a human observer.

A
direct image

B
processed image

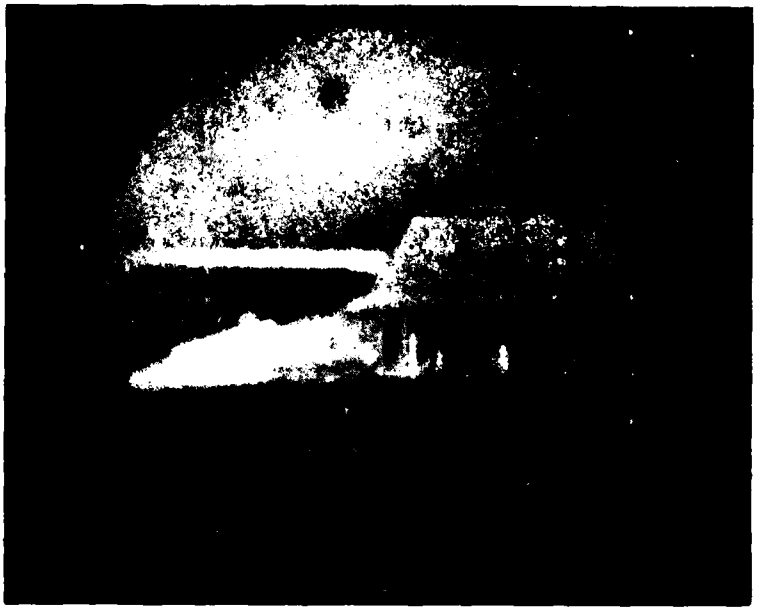

FIGURE 35. QUALITATIVE TEST WITH 3-D TARGET USING DILUTED MILK AS SCATTERING MEDIUM

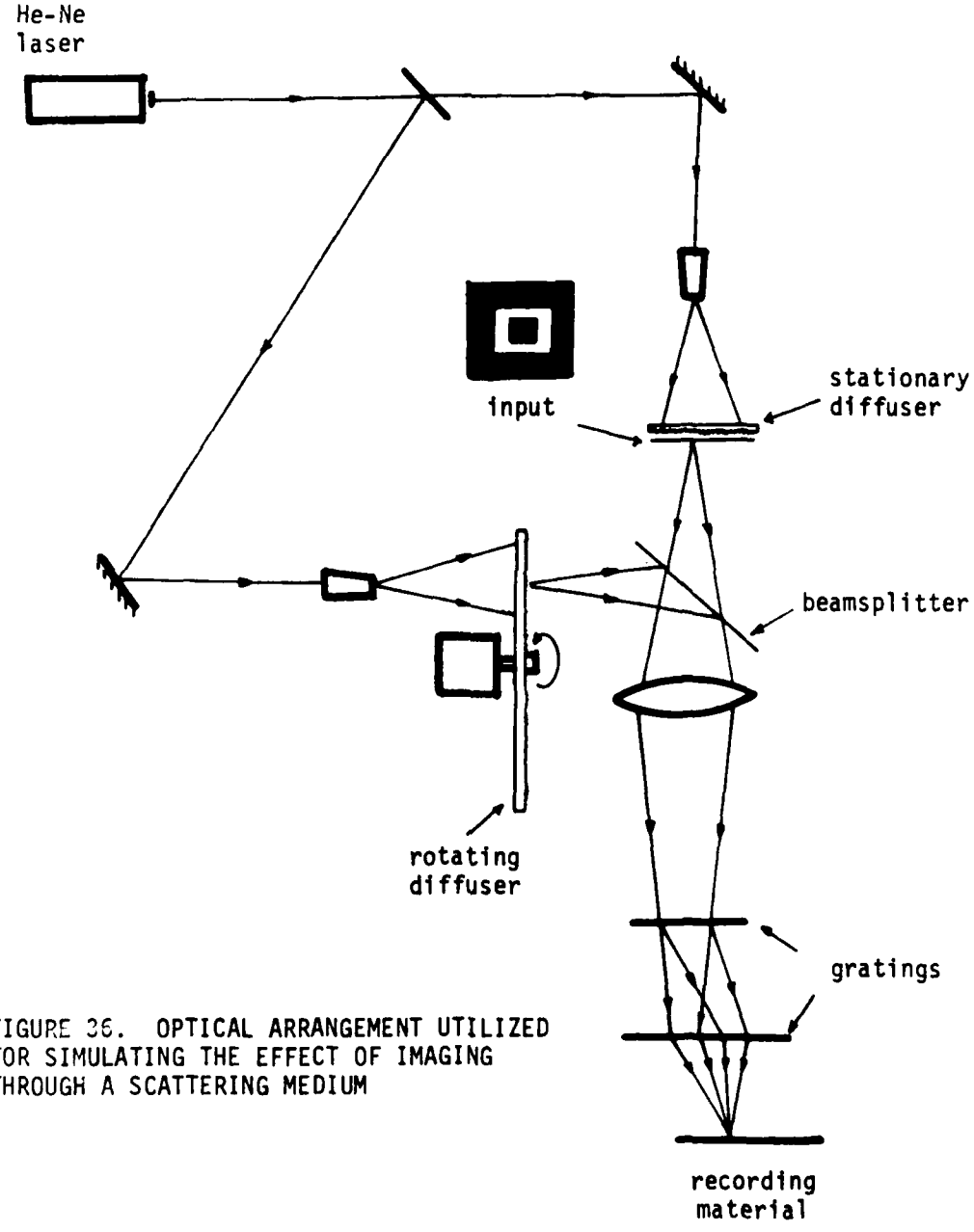

FIGURE 36. OPTICAL ARRANGEMENT UTILIZED FOR SIMULATING THE EFFECT OF IMAGING THROUGH A SCATTERING MEDIUM

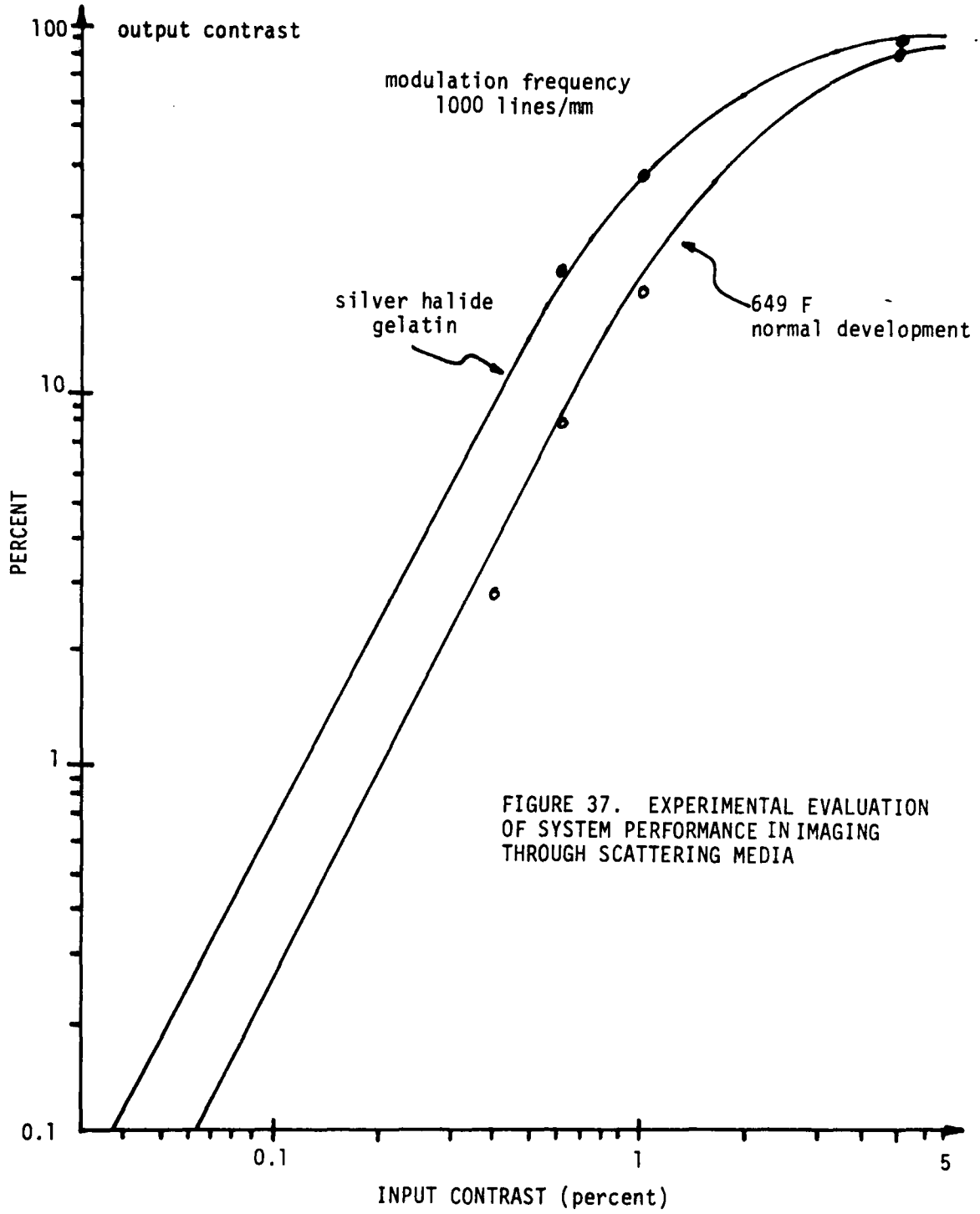

FIGURE 37. EXPERIMENTAL EVALUATION OF SYSTEM PERFORMANCE IN IMAGING THROUGH SCATTERING MEDIA

A
direct image

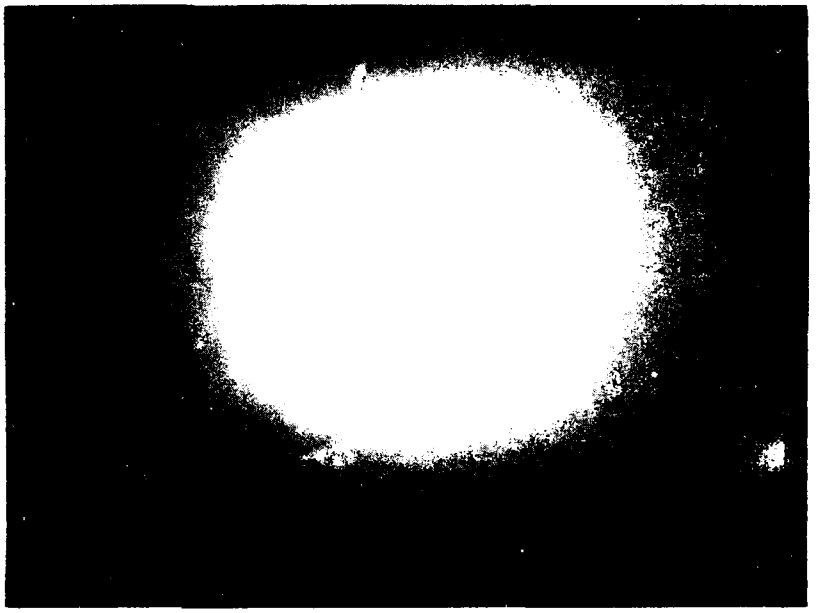

B
processed image

FIGURE 38. QUANTITATIVE TEST WITH TWO TONE TARGET

One drawback of using the 649F plate is the low diffraction efficiency for inputs with low modulation. When the intensity of the processed image is too low, other sources of noise such as detector noise and ambient noise become significant, resulting in a lower output image contrast. A common technique in improving the efficiency of recordings made with photographic materials is to bleach the emulsion[18]. The bleaching operation converts the developed opaque silver particles into transparent silver salts. While the use of bleaching techniques can improve the diffraction efficiency of the recording, the resulting SNR is invariably worse. Thus, bleaching would not be desirable in our present application.

The use of a material such as dichromated gelatin can significantly increase both the diffraction efficiency and SNR of the system. However, dichromated gelatin is far too insensitive, particularly to red light, to be used. Recently, researchers in ERIM developed a new material, the silver halide gelatin[19], which exhibits a diffraction efficiency and noise characteristic almost equal to that of dichromated gelatin. The sensitivity of the material however, is comparable to that of a photographic plate (optimum exposure is approximately 250 $\mu J/cm^2$). The processing procedure for the material for low modulation input signals has not yet been optimized. Nevertheless, our preliminary experiments indicate that a substantial improvement of the system performance can be achieved by substituting the 649F plate with this new material. In Figure 37, we show the experimental results obtained with the silver halide gelatin material together with the extrapolated performance curve. We see that the system performance is improved and the processed image would be recognizable by a human observer if the input has an image contrast of 0.17% or higher. A positive gain in image contrast can be obtained for inputs as low as 0.01%. Moreover, the processed image obtained with the silver halide gelatin material is significantly brighter. For example, for the case where the input image contrast was 0.6%, the intensity of the processed image was an order of magnitude higher than that obtained with the 649F plates

5. CONCLUSIONS AND RECOMMENDATIONS

We have introduced a grating interferometric imaging system for imaging through scattering media. The system has been demonstrated to be capable of substantially improving the image contrast. The system is shown to be relatively insensitive to normal vibration and air disturbance, making it feasible for field applications.

A better indication of the system capability is to express the performance in terms of visibility range. That is, the maximum range within which the target image is visible through a scattering medium. With the 2% minimum contrast criterion, the visibility range is related to the visibility attenuation coefficient σ_v by the relationship

$$R_v = - \ell n\left(0.02/\sigma_v\right)$$

In Figure 39, we plotted the visibility range curves for the cases with and without the use of the interferometric system. We can see that the visibility range is increased about 50%. As we have pointed out before, it requires more than a 2% image contast to recognize a complex target (e.g., a tank within a cluster of rocks). Let us assume that it requires a 5% image contrast to achieve recognition for a particular scene. The corresponding visibility ranges are also plotted in Figure 39. We find that with the 5% minimum contrast criterion, the use of the interferometric system would improve the visibility range by 80%. That is, the user would be more able to detect and recognize a hostile target at a range of at least 1.8 km compared to only a 1 km capability otherwise. In general, the more complicated the target scene, the larger will be the expected improvement in visibility range provided by grating interferometer imaging concept.

The use of an imaging grating interferometer for imaging through scattering media is an attractive and feasible concept. Supporting

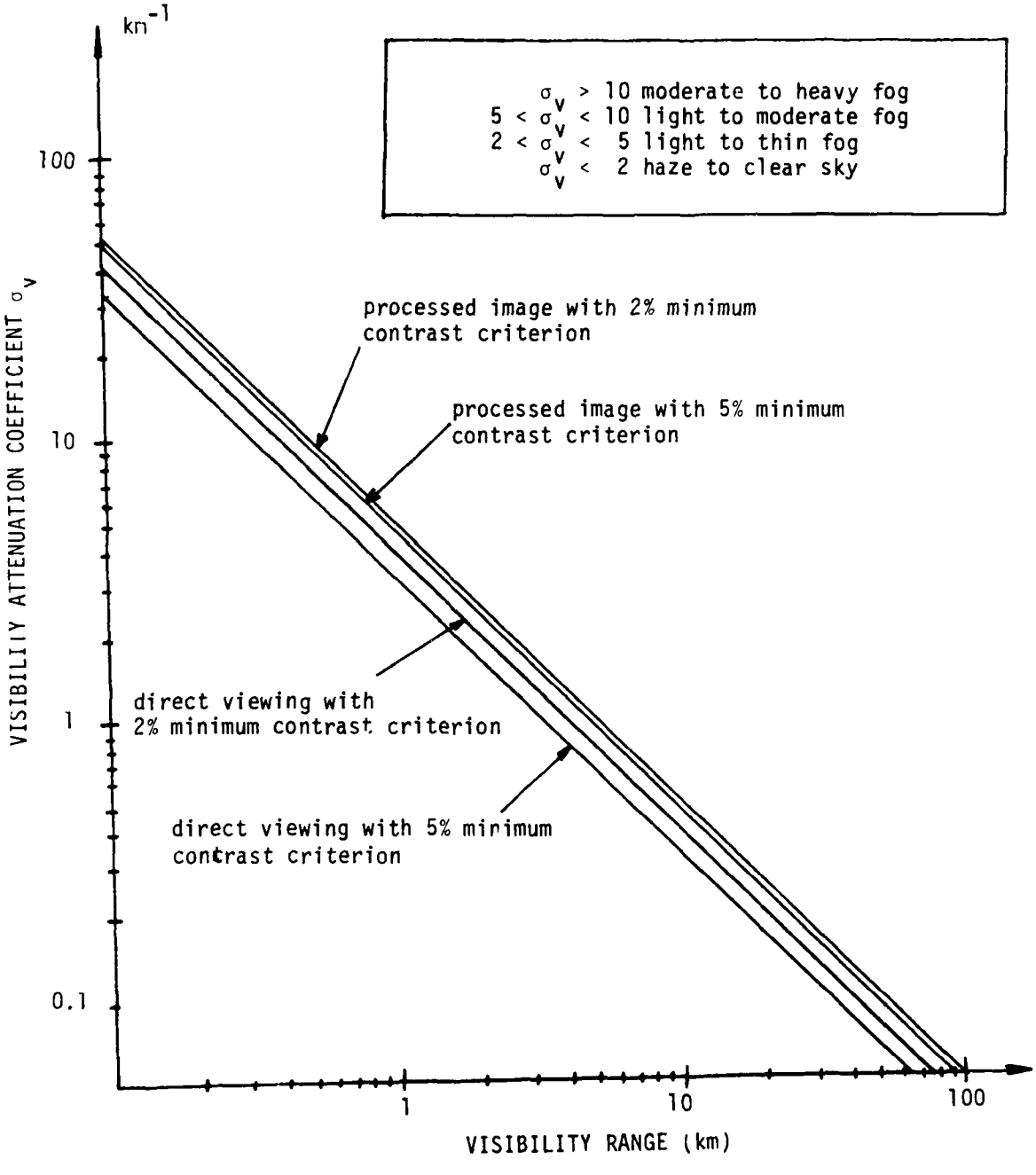

FIGURE 39. VISIBILITY RANGE AS A FUNCTION OF VISIBILITY ATTENUATION COEFFICIENT OF THE SCATTERING MEDIA

imaging experiments performed during this study utilized photographic materials as detectors. For near real time operation, a sensitive real time recording material would be required. One possible approach is to construct an image converter-intensifier in front of a real time light modulator. The image converter-intensifier would actively increase the system sensitivity and allow the use of IR illumination. An alternate approach is to detect the stationary intensity pattern produced by the unscattered light with a CCD photodetector array. The processing could be performed by electronic (analog or digital) filtering and subtraction techniques. Further work is needed to develop the concept introduced in this report into a practical, field usable real time imaging system design.

REFERENCES

1. World Meteorological Organization, "Code 4377, Horizontal Visibility at Surface," Geneva, Switzerland.

2. W.E.K. Middleton, "Vision through the Atmosphere," University of Toronto Press, Toronto, Canada, 1963.

3. B.J. Chang, R. Alferness and E.N. Leith, "Space-Invariant Achromatic Interferometers," Appl. Opt. 14, p. 1592, 1975.

4. E.N. Leith and B.J. Chang, "Image Formation with an Achromatic Interferometer," Optics Comm., 23, p. 217, 1977.

5. J.W. Goodman, "Introduction to Fourier Optics," McGraw-Hill, New York, 1968.

6. D.H.R. Vilkermerson, "Measurements of the Noise Spectral Power Density of Photosensitive Materials at High Spatial Frequencies," Appl. Opt. 9, 2080, 1970.

7. K.A. Stetson, "Holographic Fog Penetration," JOSA, 57, p. 1060, 1967. A.W. Lohmann and C.A. Schmalfuss, "Holographic Imaging through Moving Fog," Opt. Comm. 26, p. 318, 1978.

8. D.E. Duffy, "Moire Ganging of In-Plane Displacement Using Double Aperture Imaging," Appl. Opt. 11, p. 1778, 1972.

9. S. Iwasa and J. Feinleb, "The PROM Device in Optical Processing Systems," Opt. Eng., 13, p. 235, 1974.

10. T.D. Beard, W.P.Bleha and S.Y. Wong, "AC Liquid Crystal Light Valves," Appl. Phys., Letter, 22, p. 90, 1973.

11. E.B. Champagne, "A Qualitative and Quantitative Study of Holographic Imaging," Ph.D. Dissertation, Ohio State University, University Microfilms No. 67-10876, 1967.

12. M. Chang "Dichromated Gelatin of Improved Optical Quality," Appl. Opt. 10, p. 2550, 1971.

13. B.J. Chang and C.D. Leonard, "Dichromated Gelatin for the Fabrication of Holographic Optical Elements," Appl. Opt. 18, p. 2407, 1979.

14. W.S. Colburn and J.B. Dubow, "Photoplastic Recording Materials," Technical Report AFAL-TR-73-255, August 1973.

15. W.S. Colburn, L.M. Ralston, and J.C. Dwyer, "Holographic Recording in Thermoplastic at 1.15 μm," Applied Physics Letter, 23, p. 145, 1973.

16. W.H. Lee, "Computer-Generated Holograms: Techniques and Applications," Progress in Optics, Vol. 16, North-Holland, 1978.

17. R.C. Fairchild and J.R. Fienup, "Computer-Originated Hologram Lenses," Proc. SPIE, Vol. 215-01, 1980.

18. J. Upatnieks and C. Leonard, "Diffraction Efficiency of Bleached Photographically Recorded Interference Patterns," Appl. Opt. 8, p. 85, 1969.

19. B.J. Chang and K. Winick, "Silver Halide Gelatin Holograms," Proc. SPIE, Vol. 215, 1980.

20. J.R. Fienup, "Analytical Design of a Single Optical Element," ERIM Memo: EO-80-2097

DISTRIBUTION LIST

No. of Copies	Organization
12	Commander Defense Technical Info Center ATTN: DDC-DDA Cameron Station Alexandria, VA 22314
1	Commander US Army Materiel Development & Readiness Command ATTN: DRCDMD-ST 5001 Eisenhower Avenue Alexandria, VA 22333
2	Commander US Army Armament Research & Development Command ATTN: DRDAR-TSS (2 cys) Dover, NJ 07801
1	Commander US Army Armament Materiel Readiness Command ATTN: DRSAR-LEP-L, Tech Lib Rock Island, IL 61299
1	Director US Army ARRADCOM Benet Weapons Laboratory ATTN: DRDAR-LCB-TL Watervliet, NY 12189
1	Commander US Army Aviation Research & Development Command ATTN: DRSAV-E P.O. Box 209 St. Louis, MO 61366
1	Director US Army Air Mobility Research & Development Laboratory Ames Research Center Moffett Field, CA 94035
1	Commander US Army Communications Research & Development Command ATTN: DRDCO-PPA-SA Fort Monmouth, NJ 07703
1	Commander US Army Electronics Research & Development Command Technical Support Activity ATTN: DELSD-L Fort Monmouth, NJ 07703
1	Night Vision Electro Optics Laboratory ATTN: DEL-NV-AC, P. Travesky Fort Belvoir, VA 22060
1	Commander US Army Missile Command ATTN: DRSMI-R Redstone Arsenal, AL 35809
1	Commander US Army Missile Command ATTN: DRSMI-YDL Redstone Arsenal, AL 35809
1	Commander US Army Missile Command ATTN: Dr. Charles R. Christensen Redstone Arsenal, AL 35809
1	Commander US Army Tank Automotive Research & Development Command ATTN: DRDTA-UL Warren, MI 48090
1	Commander US Army Research Office ATTN: Dr.J. Mink P.O. Box 12211 Research Triangle Park, NC 27709

DISTRIBUTION LIST

No. of Copies	Organization
1	Director US Army TRADOC Systems Analysis Activity ATTN: ATAA-SL, Tech Lib White Sands Missile Range NM 88002
2	Environmental Research Institute of Michigan ATTN: Dr. Anthony M. Tai/ Dr. Carl C. Aleksoff Radar and Optics Div. P.O. Box 8618 Ann Arbor, MI 48107
1	Environmental Research Institute of Michigan ATTN: Carl D. Leonard Electro Optics Dept. P.O. Box 8618 Ann Arbor, MI 48107
1	University of Connecticut Department of Chemistry ATTN: Prof. C.E. Waring Storrs, CT 06268

No. of Copies	Organization
	Aberdeen Proving Ground
	Dir, USAMSAA ATTN: DRXSY-D DRXSY-MP, H. Cohen
	Cdr, USATECOM ATTN: DRSTE-TO-F
	Dir, CSL Bldg E3516, EA ATTN: DRDAR-CLB-PA
	Dir, CSL ATTN: E. Steubing J. Vervier Bldg E3516, EA
	Cdr, PM Smoke & Obscurants ATTN: DRCPM-SMK Bldg 324

USER EVALUATION OF REPORT

Please take a few minutes to answer the questions below; tear out this sheet and return it to Director, US Army Ballistic Research Laboratory, ARRADCOM, ATTN: DRDAR-TSB, Aberdeen Proving Ground, Maryland 21005. Your comments will provide us with information for improving future reports.

1. BRL Report Number _____

2. Does this report satisfy a need? (Comment on purpose, related project, or other area of interest for which report will be used.)

_____

_____

_____

3. How, specifically, is the report being used? (Information source, design data or procedure, management procedure, source of ideas, etc.) _____

_____

_____

4. Has the information in this report led to any quantitative savings as far as man-hours/contract dollars saved, operating costs avoided, efficiencies achieved, etc.? If so, please elaborate.

_____

_____

5. General Comments (Indicate what you think should be changed to make this report and future reports of this type more responsive to your needs, more usable, improve readability, etc.) _____

_____

_____

_____

6. If you would like to be contacted by the personnel who prepared this report to raise specific questions or discuss the topic, please fill in the following information.

Name: _____

Telephone Number: _____

Organization Address: _____

_____

_____


ATE
LME